JOURNAL OF PETROLOGY | VOLUME 55 | NUMBER 1 | PAGES 103–131 | 2014 | doi:10.1093/petrology/egt062

A Garnet–Zircon Oxygen Isotope Record of Subduction and Exhumation Fluids from the Franciscan Complex, California

F. ZEB PAGE[1,2,3]*, ERIC J. ESSENE[2]†, SAMUEL B. MUKASA[2]‡ AND JOHN W. VALLEY[3]

[1]DEPARTMENT OF GEOLOGY, OBERLIN COLLEGE, 52 W. LORAIN ST., OBERLIN, OH 44074, USA

[2]DEPARTMENT OF EARTH AND ENVIRONMENTAL SCIENCES, UNIVERSITY OF MICHIGAN, 2534 C. C. LITTLE BUILDING, ANN ARBOR, MI 48109-1007, USA

[3]WISCSIMS, DEPARTMENT OF GEOSCIENCE, UNIVERSITY OF WISCONSIN, 1215 W. DAYTON ST., MADISON, WI 53706, USA

RECEIVED MARCH 1, 2013; ACCEPTED SEPTEMBER 27, 2013
ADVANCE ACCESS PUBLICATION NOVEMBER 13, 2013

Tectonic blocks of high-grade metamorphic rock hosted by the Franciscan mélange commonly preserve textural and geochemical evidence for metasomatism and blueschist-facies overprinting within a subduction zone. These exhumation events can obscure information on the nature of subduction fluids at depth that might otherwise be preserved by these rocks in this tectonic setting. Cation and oxygen isotope zoning in garnets from eclogite and garnet–hornblende rocks with minimal textural evidence of retrogression reveals separate prograde and retrograde fluid histories. Garnet cores preserve a homogeneous prograde oxygen isotope history with both high ($\delta^{18}O$ ~11‰) and low (~4‰) values in different samples probably recording altered ocean-crust protolith compositions. Multiple episodes of garnet resorption and regrowth record a dramatically changing bulk oxygen isotope ratio resulting in 6–7‰ neoformed garnet rims with sharp core–rim boundaries in both samples. Matrix omphacite and hornblende are in profound oxygen isotope disequilibrium with garnet cores but are in equilibrium with garnet rims despite the appearance of overall textural equilibrium in thin section. This cryptic metasomatism found in samples from different locations within the Franciscan Complex brings into question existing thermobarometry on non-inclusion phases for this complex, as well as interpretations based on whole-rock geochemical data. Zircon ages and oxygen isotope equilibrium with late-forming garnet are consistent with post-metasomatic formation of zircon. The ability of garnet and zircon to record multiple fluid events and tie them to P–T–t–*fluid history is a powerful tool in gaining an improved understanding of the complex fluid environments within subduction zones.*

KEY WORDS: *subduction; ion microprobe; SIMS; oxygen isotopes; eclogite; Franciscan;* P–T–*time–fluid path*

INTRODUCTION

The relationships between the record of fluids preserved in high-pressure metamorphic rocks exhumed from subduction zones, the fluids that are presumed to be responsible for the generation of arc magmas, and the characteristic subduction-zone trace element signature, are areas of great interest in arc petrology (e.g. Bebout, 2007). Dehydration reactions within the down-going slab generate substantial fluxes of aqueous fluid that migrate into the mantle hanging wall of the subduction zone, dictating the extent to which mantle melting will occur (e.g. Peacock, 1990; Kerrick & Connolly, 2001). The record of these fluids found in exhumed subduction-zone metamorphic rocks is mixed, however. Whole-rock stable isotope and trace element data have been used to establish extensive fluid–rock interaction and metasomatism within the subduction environment (Bebout & Barton, 1989, 1993; Sorensen & Grossman, 1989), as well as mechanical mixing along the slab–mantle interface (King *et al.*, 2006, 2007; Marschall & Schumacher, 2012). Metasomatic rocks such as jadeitites and related lithologies are commonly found in serpentinite mélanges associated with subduction zones, and preserve evidence of complicated fluid histories

*Corresponding author. Present address: Department of Geology, Oberlin College, 52 W. Lorain St., Oberlin, OH 44074, USA. Telephone: +1 440 775 6701. Fax: +1 440 775 8038. E-mail: zeb.page@oberlin.edu
†Deceased. ‡Present address: College of Engineering and Physical Sciences, University of New Hampshire, Kingsbury Hall Room W 289, 33 Academic Way, Durham, NH 03824, USA.

(Johnson & Harlow, 1999; Harlow *et al.*, 2003; Sorensen *et al.*, 2006; Fu *et al.*, 2010).

Other studies, principally on eclogite and related rocks, that report textural evidence of metamorphic fluids in the form of fluid inclusions (Scambelluri & Philippot, 2001) and veins (Spandler & Hermann, 2005) suggest that these features are the products of internal fluid flow and are unlikely to represent fluid entering or leaving the subducting slab. A large number of geochemical studies are similarly suggestive of limited fluid flow in samples of mafic metamorphic rocks formed in subduction zones (Philippot & Selverstone, 1991; Selverstone *et al.*, 1992; Getty & Selverstone, 1994; Barnicoat & Cartwright, 1995; Ganor *et al.*, 1996; Putlitz *et al.*, 2000, 2001; Früh-Green *et al.*, 2001).

A commonly cited reason for these disparate results is that fluid flow within subducting slabs may be highly channelized, and the discrepancy between studies reflects the low permeability of subducted mafic rocks and the complicated mélange structure of the slab–mantle interface (Bebout & Barton, 2002; Breeding *et al.*, 2004; King *et al.*, 2006, 2007; Ague, 2007).

Additionally, the prograde and peak metamorphic geochemical record of some samples can be obscured by variable metasomatism during exhumation by channelized flow immediately above the subducting slab. Geochemical studies of metamorphic rocks that preserve evidence of substantial fluid flow and metasomatism often employ whole-rock or bulk mineral separates, an approach that homogenizes zoned minerals and makes discerning between prograde and retrograde fluids challenging. Recent detailed work on high-pressure veins from alpine eclogites suggests that these rocks can preserve a chemically distinct record of both internally and externally sourced fluids, resolvable only by preserving the spatial context of geochemical analyses (Spandler *et al.*, 2011). In addition, garnets from orogenic eclogites preserve subtle zoning in oxygen isotope ratios that records a previously unrecognized prograde fluid infiltration (Russell *et al.*, 2013).

In this study we interrogate the stable isotopic record of subduction zone metamorphism preserved in garnet and zircon at a fine (μm) scale. In addition to its wide use as a geochronometer, zircon has become highly valued for its ability to preserve a robust record of a variety of isotopic and trace-element geochemical systems through rather extreme conditions (e.g. Hanchar & Hoskin, 2003; Bowman *et al.*, 2011). Similarly, beyond its utility in thermobarometry, garnet is characterized by slow (although not as slow as zircon) intracrystalline diffusion rates, and the ability to retain geochemical information in the form of growth zoning up to granulite-facies conditions (Coghlan, 1990; Vielzeuf *et al.*, 2005; Ganguly, 2010; Page *et al.*, 2010). Zircon and garnet are both commonly found in eclogite and related subduction zone metamorphic rocks, and can record information from both the subduction and exhumation phases of metamorphism (Krogh *et al.*, 1974; Krogh, 1982; Rubatto *et al.*, 1999; Schmitz & Bowring, 2001; Page *et al.*, 2003). By analyzing oxygen isotope ratios by ion microprobe in zircon and garnet, we can use the robust nature of these minerals to see through the multiple episodes of metasomatism that might be expected in the subduction zone environment. Furthermore, by identifying the oxygen isotope record of fluids in minerals that also record pressure–temperature and geochronological information, the fluid–rock interaction history may be tied directly to the P–T–t–fluid(s) history for a more complete understanding of subduction dynamics. In doing so, for example, it may be possible to resolve the complications of widespread fluid overprinting during exhumation, and gain more insight into the nature and timing of fluid fluxes at depth in subduction zones.

Two zircon- and garnet-bearing eclogite and hornblendite samples were chosen for this study from the Franciscan Complex of central California. The Franciscan is among several paleo-subduction zones in which tectonic blocks of high-pressure metamorphic rocks are hosted by a sedimentary–ultramafic mélange. These rocks are renowned for their textural, chemical, and isotopic evidence of large fluid fluxes and metasomatism. High-grade metamorphic blocks preserve textural evidence of metasomatism in the form of glaucophane- and actinolite-rich rinds (Coleman, 1980; Horodyskyj *et al.*, 2009) as well as the presence of euhedral minerals (zoisite, aragonite, titanite, omphacite), which grew into fluid-filled cavities (Essene & Fyfe, 1967; Cloos, 1986; Page *et al.*, 2007*a*). Geochemical evidence of metasomatism in the form of zoned minerals exists both for elements typically viewed as highly mobile, such as the large ion lithophile elements (LILE; e.g. Sorensen *et al.*, 1997; Catlos & Sorensen, 2003), and those that are generally thought to be less soluble in aqueous solution, such as high field strength elements (HFSE) and the light rare earth elements (LREE; e.g. Sorensen & Grossman, 1989). To maximize the potential for recording both an early and late history of subduction fluids, a sample was chosen that contains garnets that record a prograde subduction history, and a second sample with garnet that records the oldest ages in the region.

REGIONAL GEOLOGY

The high-grade metamorphic rocks hosted by the Franciscan Complex in the Central and Northern California Coast Ranges have been the subject of intensive petrological and geochronological study for the past century. High-grade blocks (usually on the scale of 1–10 m) of eclogite, blueschist and garnet hornblendite (sometimes referred to as amphibolite despite the common lack of plagioclase) are hosted by a lower-grade metagreywacke mélange (e.g. Bailey *et al.*, 1964; Cloos, 1986). Many high-grade blocks preserve a polymetamorphic history with

evidence of significant rock–fluid interaction. A ubiquitous blueschist-facies overprint on all lithologies was recognized from the onset of petrological investigation in the area (e.g. Holway, 1904; Borg, 1956). Evidence of high-*P* and high-*P*/*T* overprinting (Essene & Fyfe, 1967; Moore, 1984; Moore & Blake, 1989) ultimately culminated in the proposal of counter-clockwise *P–T* paths for several eclogite blocks (Oh & Liou, 1990; Wakabayashi, 1990; Krogh *et al.*, 1994). More recently, a series of studies have applied quantitative thermobarometry to inclusion phases in garnet from eclogite, generating a robust set of counter-clockwise *P–T* paths, with near-peak conditions of ~600°C and ~24 kbar, and blueschist-facies prograde paths (Ravna & Terry, 2004; Tsujimori *et al.*, 2006*a*; Page *et al.*, 2007*a*).

Isotopic dating of Franciscan metamorphic rocks has been continuing for almost 50 years, and many of these studies have been summarized by Wakabayashi & Dumitru (2007). Garnet hornblendites yield the oldest ages (hornblende Ar–Ar, 156–160 Ma; Ross & Sharp, 1986, 1988; Wakabayashi & Dumitru, 2007; garnet Lu–Hf, 153–168 Ma; Anczkiewicz *et al.*, 2004). Garnet Lu–Hf mineral isochrons for eclogite (~158 Ma) and blueschist (~147 Ma) blocks yield generally younger ages than those for hornblendite, suggesting that the three high-grade lithologies in the Franciscan record the slow cooling of the subduction zone (Anczkiewicz *et al.*, 2004). $^{40}Ar/^{39}Ar$ ages of phengite in Franciscan high-grade blocks generally cluster around 135–140 Ma, but range up to 156 Ma; phengite grains with younger ages are generally texturally late, whereas older phengite (e.g. 156 Ma from the Tiburon eclogite; Catlos & Sorenson, 2003) is apparently texturally in equilibrium with the eclogitic assemblage. Most phengite grains are variably enriched in the LILE, principally Ba (Sorensen *et al.*, 1997; Catlos & Sorensen, 2003; Page *et al.*, 2007*a*). The wide range in their ages has been proposed as evidence for long-lived fluid metasomatism within the Franciscan subduction zone (Catlos & Sorenson, 2003). A lawsonite Lu–Hf isochron yielded an age of 146 Ma for a blueschist block from Tiburon, consistent with other ages from blueschist blocks (Mulcahy *et al.*, 2009). Nelson (1991) found similarly young ages from blueschist minerals in late veins and vugs in eclogite from Tiburon and the Diablo Range, with an Rb–Sr isochron of ~150 Ma. In summary, $^{40}Ar/^{39}Ar$ and Lu–Hf ages from prograde and peak minerals in eclogite and hornblendite range from 153 to 168 Ma. Rb–Sr ages on late vug minerals, the $^{40}Ar/^{39}Ar$ chronology of texturally late phengite, and Lu–Hf ages for garnet and lawsonite in blueschists range from ~135 to 150 Ma (Nelson, 1991). These younger blueschist-facies ages overlap $^{40}Ar/^{39}Ar$ phengite ages from coherent regions of Franciscan metamorphic rocks (120–154 Ma; Wakabayashi & Dumitru, 2007).

SAMPLE DESCRIPTIONS

Two high-grade metamorphic blocks were chosen for this study. The first block is an eclogite located ~5 km SW of Healdsburg, California (38°35′42″N, 122°53′50″W), known as the Junction School (JS) eclogite (Sorensen *et al.*, 1997; Page *et al.*, 2007*a*). The sample in this study is from an ~15 m diameter tectonic block, the largest and least visibly overprinted block at this locality. This block was chosen for study because it appears to be a relatively pristine sample of Franciscan eclogite with minimal evidence of overprinting in the form of significant veining or abundant late glaucophane; it does not have a metasomatic rind. The JS sample is a fine- to medium-grained eclogite consisting primarily of <1 mm omphacite and 0·5–1 mm garnet grains (Fig. 1a). A detailed textural and mineralogical description of this rock has been given by Page *et al.* (2007*a*) and is therefore presented here only in summarized form. Both omphacite and garnet are compositionally zoned, and this zoning is visible in backscattered electron (BSE) images (Fig. 1b and c). Large matrix rutile crystals (500–1000 μm) are partially to completely replaced by titanite (Fig. 1a). In more overprinted samples, partially resorbed garnets are rimmed by chlorite, phengite, and minor glaucophane. The outcrop has a mottled appearance on the centimeter scale, with darker patches containing a higher percentage of chlorite and phengite; joints in the rock contain abundant phengite (Sorensen *et al.*, 1997). In thin section, more heavily altered patches contain euhedral epidote and omphacite crystals that may have originally grown into fluid-filled cavities (Page *et al.*, 2007*a*), and are now surrounded by quartz (Fig. 1c) or titanite. Garnets in these areas are strongly zoned and show evidence for multiple episodes of growth and resorption. Abundant small zircons are found in garnet and omphacite rims (Fig. 1b and c). Mineral inclusions in garnet cores record the prograde metamorphism of this sample from ~10 kbar and 400°C to a peak of ~22 kbar and 550°C preserved in garnet mantles within a clear resorption boundary (Page *et al.*, 2007*a*). Garnet rims record blueschist-facies conditions of 10–16 kbar and 350–400°C; although the prograde and retrograde *P–T* path of this rock is known in some detail, it has not yet been the subject of any geochronological studies.

The second sample is plagioclase-free garnet hornblendite from Panoche Pass (PNP) in the Diablo Ranges ~40 km SE of Hollister, California (36°39′29″N, 121°06′48″W); it is composed of brown hornblende (0·5–2 mm long), garnet (1–3 mm) and ilmenite–rutile compound grains (~300 μm, Fig. 1d and e). Hornblendite from the Panoche Pass locality was described by Hermes (1973), and the region has recently been mapped in detail by Wakabayashi & Dumitru (2007). Brown or green amphibole (hornblende) cores are surrounded by thin blue amphibole rims (Fig. 1d), and contain abundant

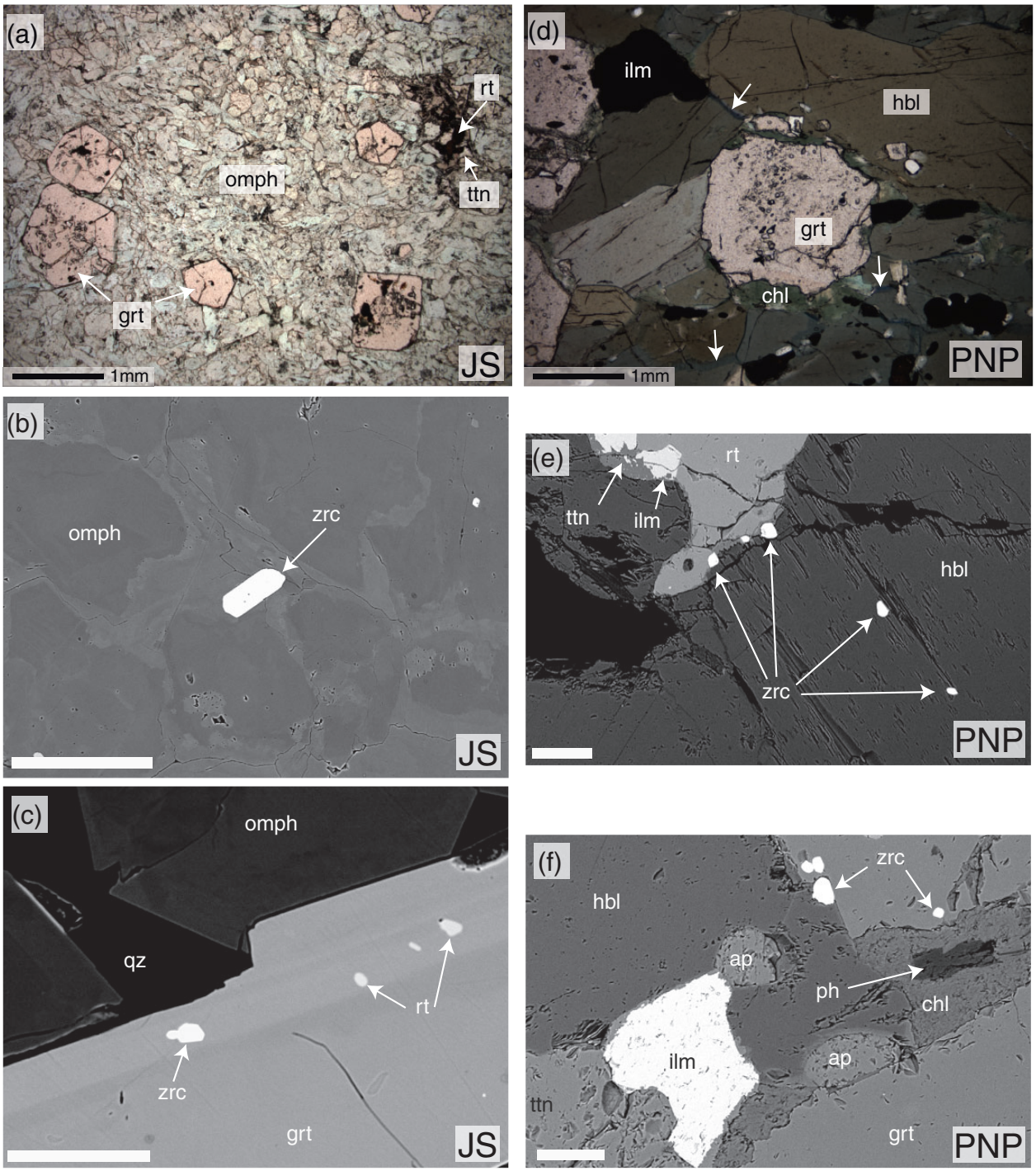

Fig. 1. Representative photomicrographs (a, d, plane-polarized light) and BSE images (b, c, e, f) of the Franciscan eclogite and hornblendite blocks in this study. Scale bars represent 200 μm unless otherwise noted. (a–c) Junction School (JS) eclogite. (a) Omphacite (omph) + garnet (grt) + rutile (rt). Late titanite (sph) rims rutile. (b) Zoned omphacite with bright, high-Fe^{3+} rims surrounding slightly rounded zircon (zrc). (c) Zoned garnet with inclusions of zircon and rutile in brighter rim. Late quartz (qz) forms polygonal contacts with omphacite. (d–f) Panoche Pass (PNP) hornblendite. (d) Hornblende (hbl) + garnet (grt) + ilmenite (ilm). Thin bluish amphibole rims and late veins are indicated by white arrows. (e) Small zircons occur as inclusions in hornblende and also decorate rutile and hornblende grain boundaries. Late titanite appears to have formed at the expense of ilmenite and rutile. (f) Late chlorite (chl) and phengite (ph) filling an embayment in garnet. Small zircons decorate the edge of the garnet, and occur as inclusions in the garnet rim. ap, apatite.

inclusions of apatite (Fig. 1e and f). Cation zoning in garnets is not as dramatic as in the JS eclogite. Garnet has resorbed rims and abundant inclusions of hornblende, apatite, rutile, ilmenite and quartz. Ilmenite is often found in compound grains with rutile that has thin rims of titanite (Fig. 1e and f). Secondary compositionally zoned allanitic epidote, titanite, apatite, phengite, glaucophane and chlorite decorate grain boundaries, particularly around partially resorbed garnet (Fig. 1f). This block was chosen for study because it has one of the best-constrained chronologies of any Franciscan block. Garnet in this block crystallized at 168·7 ± 0·8 Ma (Lu–Hf; Anczkiewicz *et al.*, 2004) and hornblende at 162 ± 2 Ma, with retrograde muscovite forming at ~145 Ma (Ar–Ar; Ross & Sharp, 1988). Existing thermobarometric estimates are restricted to garnet–hornblende thermometry, yielding temperatures of 650–750°C (Anczkiewicz *et al.*, 2004).

ANALYTICAL METHODS

Most chemical and isotopic analyses in this paper were performed on polished thin sections to preserve textural information. However, given the scarcity of relatively large zircon grains in these lithologies, zircons were separated and concentrated using standard gravimetric and magnetic techniques, followed by handpicking and mounting in epoxy. BSE and polychromatic cathodoluminescence (CL) images of minerals were made using the CAMECA SX100 electron microprobe at the University of Michigan and scanning electron microscopes at the University of Wisconsin–Madison and Oberlin College. Mineral chemistry was determined on a CAMECA SX100 electron microprobe at the University of Michigan using a focused 15 kV, 10 nA electron beam. Natural and synthetic silicate and oxide standards were used, and data were reduced using a CAMECA PAP-type correction calculating oxygen by stoichiometry.

Laser fluorination

Small-diameter (6 mm × ~10 mm) plugs were drilled from hand samples of eclogite and hornblendite and were crushed to pieces of ~0·5 mm in diameter. Garnet, clinopyroxene, hornblende and titanite separates were handpicked, and chips for analysis were selected for optical clarity and lack of visible inclusions or attached contamination. Aliquots of mineral chips weighing 1–2 mg were pre-treated overnight in the sample chamber with BrF_5, then individually heated with a CO_2 laser in the presence of BrF_5. Samples of whole-rock powder were not pre-treated in BrF_5 to avoid pre-reaction, but instead were evacuated overnight in an airlock chamber and individually moved under vacuum to the fluorination chamber for analysis (Spicuzza *et al.*, 1998). All analyses were standardized against four analyses of oxygen isotope standard UWG-2 per day ($\delta^{18}O = 5{\cdot}80‰$ VSMOW; Valley *et al.*, 1995) and reported in standard per mil (‰) notation relative to VSMOW. The eight analyses of UWG-2 averaged 5·79 ± 0·14‰ (2 SD; 2 days of analyses), yielding an average correction of 0·01‰.

Ion microprobe

Separated zircons were mounted within 5 mm of the center of a 25 mm epoxy disk with standards AS3 (Paces & Miller, 1993; Schmitz *et al.*, 2003) and 91500 (Wiedenbeck *et al.*, 1995, 2004) and polished to the approximate centers of the sample grains. After initial CL and BSE characterization, zircon was analyzed for U–Th–Pb elemental ratios and Pb isotopic composition (details below). Correlation of U–Pb, trace element and oxygen isotope analyses followed a similar approach to that described by Cavosie *et al.* (2006). After U–Pb analysis, zircons were imaged with secondary electrons (SE) and CL to determine exact pit locations. Trace element analyses were made on the same surface as U–Pb analyses, typically within the same CL domain. After trace-element analysis, oxygen isotope standard KIM-5 zircon (Valley, 2003) was face-mounted into the existing disk and flattened and polished by hand. Care was taken to remove the least amount of material possible and to minimize any differential polishing relief between zircon and epoxy matrix as this can affect precision in oxygen isotopic analysis (Kita *et al.*, 2009). After polishing to remove existing analysis pits, zircons were then re-imaged in CL, and $\delta^{18}O$ analyses were targeted to the same CL zones as previous analyses, and in many cases directly underlie previous analysis spots.

Garnet and quartz were analyzed in polished thin section by grinding the section into a 25 mm circle, with the target grain or grains within 5 mm of the center. Oxygen isotope standards UWG-2 (garnet; Valley *et al.*, 1995) and UWQ-1 (quartz; Kelly *et al.*, 2007) were epoxied into small holes drilled near the center of the round thin sections, and polished to be co-planar with the sample surface. One highly zoned garnet from the JSE was located at the extreme edge of a rectangular thin section, and so an ~7 mm × 7 mm square portion of the thin section containing the garnet was cut out and remounted at the center of a new epoxy mount containing UWG-2 and UWQ-1; sample and standard were also polished to be co-planar in this case.

U–Pb analyses were made using the CAMECA ims-1270 ion microprobe at the W. M. Keck Foundation Center for Isotope Geochemistry National Ion Microprobe Facility, University of California, Los Angeles. Analyses were guided by CL images of zircons and were made using an ~30 μm diameter beam, and instrument conditions as described by Quidelleur *et al.* (1997). Rare earth elements (La–Lu) and other selected trace elements (Ti, P, Y, Hf, Th and U) were measured using a CAMECA ims-1280 ion microprobe at the WiscSIMS Laboratory, Department of Geoscience, University of Wisconsin–Madison, using an

~4 nA O^- primary ion beam (23 kV total accelerating voltage) shaped to a diameter of 20–25 μm on the sample surface. Analyses were conducted in monocollection mode using the axial ETP electron multiplier, applying a combination of energy filtering (40 eV) and high mass resolution (mass resolving power of 5000) as described by Page *et al.* (2007*b*).

Oxygen isotope ratios were measured at the WiscSIMS Laboratory, using the method described by Kita *et al.* (2009) and Valley & Kita (2009). Analyses were conducted using a focused 2·8–3·9 nA primary Cs^+ beam with a spot size of ~10 μm. Data were acquired during three separate analytical sessions. Two to four analyses of zircon standard KIM-5 ($\delta^{18}O = 5{\cdot}09\%$ VSMOW; Valley, 2003), garnet standard UWG-2 ($\delta^{18}O = 5{\cdot}80\%$ VSMOW; Valley *et al.*, 1995), or quartz standard UWQ-1 ($\delta^{18}O = 12{\cdot}33\%$ VSMOW; Kelly *et al.*, 2007) were performed before and after every 10–12 sample analyses. The average value of the standards bracketing each block of unknowns was used to correct for instrumental bias using the method outlined by Kita *et al.* (2009). The external precision, defined as the spot-to-spot reproducibility of the standards before and after a given set of samples, is assigned to the bracketed sample analyses. Precision for zircon analyses ranges from 0·17 to 0·32‰ (2 SD), and for quartz analyses ranges from 0·16 to 0·35‰ (2 SD). The full ion microprobe datasets for oxygen isotope analyses, including both sample and standard data, can be found in Supplementary Data Electronic Appendices 1–3 (available for downloading at http://www.petrology.oxfordjournals.org).

Oxygen isotope analysis of garnet, with its multiple solid solutions, must also be corrected for compositional bias. This bias in Fe^{3+}-poor garnets, such as those in this study, can be modeled successfully given current analytical uncertainty as a function of grossular content (Page *et al.*, 2010). Garnet samples were corrected following this method using both UWG-2 and a set of secondary garnet standards that compositionally bracket the sample. Secondary standards were analyzed during the same analytical sessions as sample garnets and calibration curves were developed for each session (Electronic Appendix 2). To apply the calibration curves to correct for compositional bias, the cation composition of the sample garnets was determined adjacent to each ion microprobe pit using the CAMECA SX51 electron microprobe at University of Wisconsin–Madison. Garnets were analyzed in point beam mode with an accelerating potential of 15 kV and 20 nA beam current. The counting time was 10 s on peak and 5 s on both sides, off-peak. Natural and synthetic silicate and oxide standards were used. Data were reduced using the Probe for Windows software (Donovan *et al.*, 2009), and oxygen was calculated by stoichiometry. The content (mol %) of garnet end-members for each ion microprobe analysis pit is reported alongside the isotopic data in Electronic Appendix 1. The matrix bias for garnets from the JS eclogite ranges from 0·9 to 1·4‰ relative to UWG-2, and the bias for garnets from the PNP hornblendite ranges from 0·8 to 1·2‰ relative to UWG-2. These corrections are substantially smaller than those required for zoned Ca- and Fe^{3+}-rich skarn garnets, and are much smaller than the isotopic zoning observed within the sample garnets. Analytical precisions from repeated analysis of the UWG-2 standard range from 0·17 to 0·42‰ (2 SD), and are added in quadrature with uncertainties in the correction scheme of ~0·3‰ (Page *et al.*, 2010), yielding a combined measure of precision and accuracy of ion microprobe analysis of oxygen isotopes in garnet ranging from 0·34 to 0·51‰ (2 SD).

RESULTS

Zoned garnet

Junction School

Garnets from the JS eclogite are characterized by prograde zoning and, in some cases, dramatic evidence of multiple episodes of resorption and regrowth. The degree of retrograde zonation varies on the thin-section scale. Figure 2 shows compositional images and a cation and oxygen isotope traverse of a retrogressed garnet (JS-1) from the JS eclogite. In high-contrast BSE images (Fig. 2a) the average atomic number ($\bar{Z}$) of the garnet can be seen to decrease slowly from the core of the garnet until there is a sharp decrease in $\bar{Z}$ ~70 μm from the rim. An X-ray map (Fig. 2b) and compositional traverses (Fig. 2c) show that the garnet has a Mn-rich center ($Alm_{57}Grs_{27}Pyp_6Sps_{10}$) with a characteristic bell-shaped Mn prograde zoning profile coupled with slowly increasing Fe and Mg contents and relatively constant Ca concentrations ($Alm_{60}Grs_{27}Pyp_{12}Sps_1$) in the center region of the garnet. Representative cation analyses from this traverse are presented in Table 1. This core region contains inclusions of phengite and omphacite that together with the zoned garnet record prograde pressures and temperatures (Page *et al.*, 2007*a*). The discontinuity between the prograde core region and the adjacent low-$\bar{Z}$ annulus is undulatory and contains deep embayments into the garnet core, indicating a period of garnet dissolution (Fig. 2a). The low-$\bar{Z}$ annulus itself is characterized by a sharp increase in Mn and decrease in Fe ($Alm_{54}Grs_{29}Pyp_{13}Sps_4$), and fills in a portion of the resorbed garnet. The outer margin of the low-$\bar{Z}$ annulus is another sharp compositional discontinuity leading to a high-$\bar{Z}$ annulus that records a spike in Fe, a decrease in Ca and Mg, and a drastic reduction in Mn ($Alm_{65}Grs_{27}Pyp_8Sps_0$). This high-Fe region appears to have filled much of the remaining resorbed garnet, and renewed growth along crystal faces (Fig. 2a). The inner portion of the high-$\bar{Z}$ annulus contains inclusions of phengite

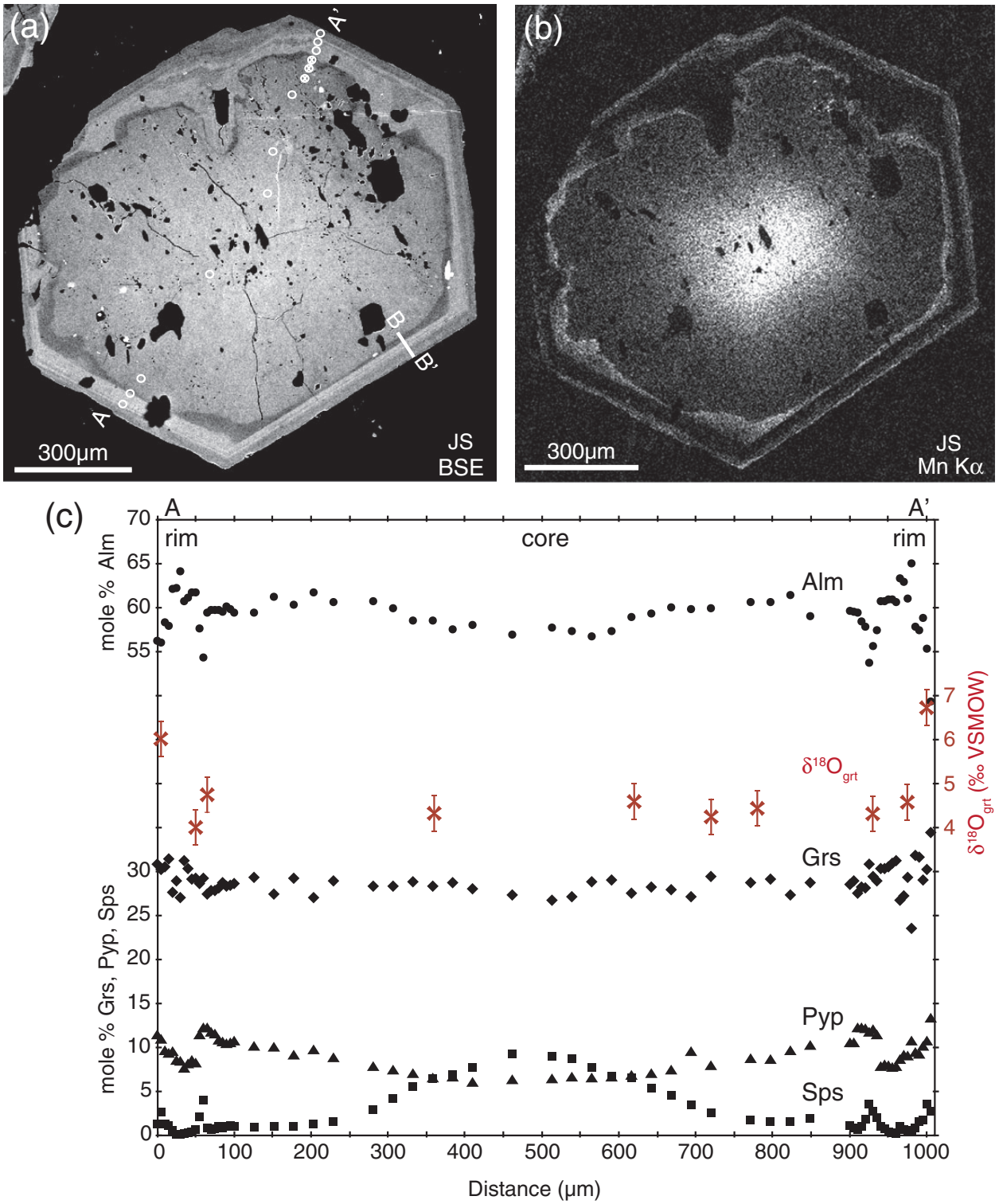

Fig. 2. Zoned garnet JS-1 from the Junction School eclogite. (a) High-contrast BSE image of a section through the approximate center of the garnet with a relatively homogeneous core composition with a thin (~70 μm) rim characterized by abrupt changes in composition. Ion microprobe pits used to measure $\delta^{18}O$ on the traverse A–A′ are shown as white circles, pits that were excluded due to overlap with inclusions are marked with an "x". Numerous quartz, epidote, phengite, and omphacite inclusions and matrix omphacite appear black; rutile inclusions are white. Small white bar at the lower right of the garnet denotes the location of the traverse B–B′ in Fig. 3. (b) Mn Kα X-ray map of the same garnet showing higher Mn concentration (bright, ~10% spessartine) in the core decreasing towards the rim with two higher-Mn annuli demarcating the inner and outer edges of the rim zone, and corresponding to low-Z regions (darker) in the BSE image. Inclusions of omphacite and phengite in the low-Mn annulus in the rim yield blueschist-facies pressures and temperatures (Page *et al.*, 2007*a*). (c) Electron- and ion-microprobe traverse A–A′ shown in (a). Ion microprobe $\delta^{18}O$ data are shown as crosses. Analytical precision is shown at the 2 SD level with bars when it is larger than the data points.

Table 1: Correlated cation and ion microprobe $\delta^{18}O$ analyses of zoned garnets from the Junction School eclogite and Panoche Pass hornblendite

	JS-1 core center Fig. 2, 620 μm*	JS-1 core mantle Fig. 2, 720 μm	JS-2 low-*Z* annulus Fig. 3	JS-2 high-*Z* annulus Fig. 3	JS-1 rim Fig. 1, 1000 μm	PNP-1 core center Fig. 4, 663 μm	PNP-2 core edge Fig. 5	PNP-2 recrystallized zones Fig. 5	PNP-1 low-*Z* annulus Fig. 4, 962 μm	PNP-1 high-*Z* rim Fig. 4, 981 μm
SiO_2	37·71	37·85	38·32	37·77	37·84	38·07	38·20	38·02	37·91	37·90
TiO_2	n.a.	n.a	0·02	0·10	n.a	n.a.	n.a.	n.a.	n.a.	n.a.
Al_2O_3	21·34	21·58	21·57	21·21	21·47	21·54	21·63	21·66	21·86	21·78
Cr_2O_3	n.d.	0·02	0·01	0·01	n.d.	0·01	n.d.	n.d.	0·05	0·01
FeO	26·07	26·68	25·02	29·12	27·34	28·08	26·88	27·87	25·06	26·31
MnO	3·09	0·90	1·86	0·11	0·12	1·67	1·06	0·59	2·65	2·77
MgO	1·73	2·06	3·15	2·13	2·31	2·30	3·10	3·11	3·50	4·13
CaO	9·83	10·81	10·52	9·60	10·25	9·12	8·98	8·73	9·02	7·35
Total	99·77	99·90	100·48	100·05	99·33	100·80	99·84	99·98	100·06	100·26
Si	3·01	3·00	3·00	3·00	3·01	3·00	3·02	3·00	2·98	2·97
Al	2·00	2·01	1·99	1·99	2·01	2·00	2·01	2·02	2·02	2·01
Ti	n.d	n.d.	n.d.	0·01	n.d	n.d	n.d.	n.d.	n.d.	n.d.
Fe^{2+}	1·74	1·77	1·64	1·93	1·82	1·85	1·78	1·84	1·65	1·73
Cr	n.d.	n.d.	n.d.	n.d.	n.d.	n.d.	n.d.	n.d.	n.d.	n.d.
Mn	0·21	0·06	0·12	0·01	0·01	0·11	0·07	0·04	0·18	0·18
Mg	0·21	0·24	0·37	0·25	0·27	0·27	0·36	0·37	0·41	0·48
Ca	0·84	0·92	0·88	0·82	0·87	0·77	0·76	0·74	0·76	0·62
O (calc)	12·01	12·01	11·99	12·00	12·02	12·00	12·02	12·01	11·99	11·98
Alm	58·1	59·1	54·4	64·2	61·1	61·6	59·8	61·7	55·0	57·3
Pyp	6·9	8·1	12·2	8·4	9·2	9·0	12·3	12·3	13·7	16·1
Grs	28·1	30·6	29·3	27·1	29·4	25·6	25·6	24·7	25·2	20·5
Sps	7·0	2·0	4·1	0·2	0·3	3·7	2·4	1·3	5·9	6·1
$\delta^{18}O$	4·5	4·2	3·7	3·9	6·7	10·9	11·5	9·5	11·2	6·7

Normalized to 8 cations; all Fe = Fe^{2+}; n.d., not detected; n.a., not analyzed; $\delta^{18}O$ analyzed by ion microprobe and reported in ‰, VSMOW.
*Figure and position along traverse (if appropriate) showing location of analysis.

and omphacite that when combined with the host garnet yield blueschist-facies pressures and temperatures (Page *et al.*, 2007*a*). Outside the high-*Z* annulus, a final intermediate-*Z* stage is visible (Fig. 2a). This outermost rim is characterized by a decrease in Fe and rise in Ca ($Alm_{59}Grs_{29}Pyp_{10}Sps_2$), and the reappearance of some Mn (Fig. 2b and c).

BSE images of the garnet rims record an even more complex story at a spatial resolution smaller than the 5 μm steps of the outer 100 μm of the traverse in Fig. 2c. Figure 3 shows a 1 μm step traverse performed on a rim section (Fig. 2a, B–B′) showing high variability. The inner margin of the low-*Z* annulus is defined by a peak of Mn and Ca that matches the sudden decrease in Fe content. The decrease of Mn that follows the peak is mirrored by an increase in Fe. The high-*Z* annulus is marked by an initial increase in Fe and decrease in Mg; Mg thereafter increases steadily towards the rim. BSE variation within both the high-*Z* annulus and the rim appear to be controlled by complementary fluctuations in Ca and Fe content, and the reappearance of Mn at the outermost (intermediate-*Z*) rim.

The Junction School eclogite garnets are also zoned in their oxygen isotope composition. Oxygen isotope data from both garnets analyzed are summarized in Table 2, with representative analyses of the different zones in Table 1. All analyses can be found in Electronic Appendix 1. Although the locations of the isotopic analyses were guided by BSE images and X-ray maps, analysis locations were chosen on a reflected light image of an Au-coated

Table 2: Summary of ion microprobe $\delta^{18}O$ analyses from the Junction School eclogite and Panoche Pass hornblendite measured at WiscSIMS

	$\delta^{18}O$ (‰,VSMOW)				
Sample	Average	2 SD	Max.	Min.	*n*
JS eclogite (JS-1 and -2)					
garnet core	4·3	0·5	4·7	3·8	12
garnet low-*Z* annulus	3·7	0·4	4	3·4	4
garnet high-*Z* annulus	4·3	1·0	5·5	3·8	10
garnet rim	6·4	1	7·2	5·8	19
zircon core	4·6	0·6	5	4·3	5
zircon rim	6·4	0·5	6·7	6·2	8
matrix quartz	25·4	0·1	25·5	25·4	4
PNP hornblendite (PNP-1, -2, -3)					
garnet core	11·3	0·5	11·7	10·9	22
garnet recrystallized	9·1	0·8	9·3	8·4	8
garnet rim	6·6	0·4	6·8	6·2	11
zircon	8·2	1·1	9·5	7·3	22

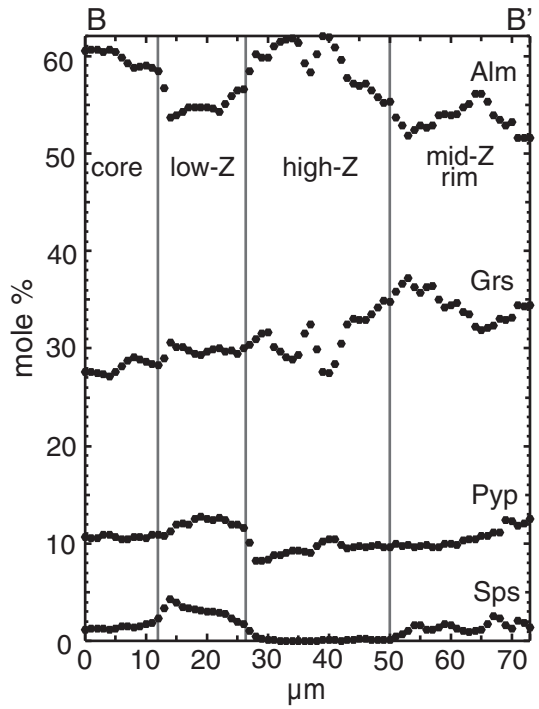

Fig. 3. Junction School eclogite garnet rim zoning. Detailed (1 μm step) compositional traverse of garnet JS-1 rim (B–B′ in Fig. 2a). Vertical lines denote the approximate boundaries of the zones as outlined in the text. The anti-correlated oscillatory behavior of Fe (Alm) and Ca (Grs) should be noted.

sample, leading to occasional analyses of inclusion-bearing regions (recognized by SEM after analysis, data excluded) and mixtures between garnet zones (included). The core region of garnet JS-1 (Fig. 2c) is homogeneous in $\delta^{18}O$ within analytical error (4·3 ± 0·5‰, 2 SD, $n = 5$). Analyses made in the low-*Z* annulus (Traverse A–A′ in Fig. 2c at 50 μm, 4·0‰) and the high-*Z* annulus (930 μm, 3·9‰; 975 μm, 4·3‰) yield identical (within error) results to each other and the core analyses. The outermost two points on this traverse yielded substantially higher $\delta^{18}O$ of 6·7‰ (at the end of the traverse) and a mixed analysis (a combination of the outermost rim and high-*Z* annulus) yielding 6·0‰ at the beginning of the traverse.

To better constrain the nature of isotopic zoning in the garnet rims, a number of analyses were made on a second garnet (JS-2) from the same sample and are shown superimposed on a high-contrast BSE image in Fig. 4. This garnet records a very similar cation zoning pattern to JS-1, with low- and high-*Z* annuli filling embayments in the partially resorbed core region. Similar 2–3 μm scale oscillations in BSE are visible within the high-*Z* annulus. Unlike JS-1, a small embayment into the high-*Z* annulus can be seen (Fig. 4) that suggests another period of resorption within the high-*Z* annulus. Multiple small ion microprobe traverses were made in this region to better constrain the rim $\delta^{18}O$. The $\delta^{18}O$ zonation of this garnet is broadly similar to that observed in garnet from sample JS-1. The $\delta^{18}O$ value of the core, low-*Z* annulus, and inner portion of the high-*Z* annulus are identical within analytical error (3·7–4·2‰, $n = 10$) with the exception of one point (5·5‰). Analyses made in the intermediate-*Z* rim and immediately outside the resorption line (where visible) in the high-*Z* annulus have substantially higher and more variable $\delta^{18}O$ (5·6–7·2, $n = 12$), with one mixed analysis yielding intermediate results (5·1‰). It is clear that the rim is higher in $\delta^{18}O$ value, but it is difficult to ascertain the fine details of the spatial pattern. Higher values appear to cluster in the middle of the rim with lower values towards the inner and outer margins, suggesting either that $\delta^{18}O$ varies across single growth zones or at a scale smaller than the 10 μm spot diameter. Taken together, these garnets preserve in their cation chemistry a history of at least two periods of dissolution and regrowth. Garnet cores and annuli record homogeneous oxygen isotope ratios throughout their early history, with a significant increase in $\delta^{18}O$ recorded in the outermost rims that crystallized after the second resorption episode.

Panoche Pass

Cation zoning in the Panoche Pass hornblendite garnet is less variable than the Junction School eclogite. BSE imaging (Fig. 5a) records somewhat patchy zoning in the garnet core, with a brighter center and darker outer

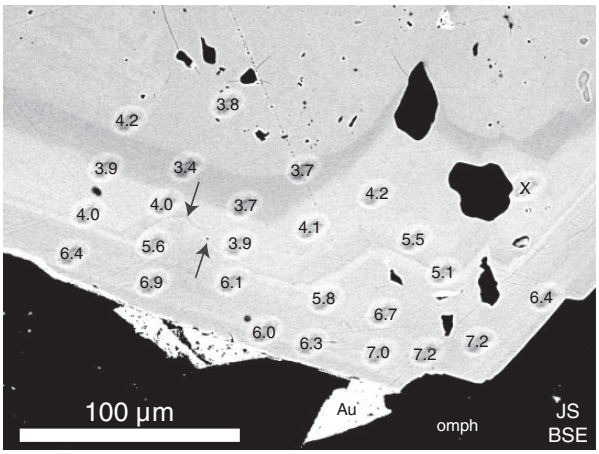

Fig. 4. High-contrast BSE image of garnet JS-2 rim. Evidence of a second period of resorption is visible within the high-Z annulus and is indicated with black arrows. The extremely bright high-Z patches outside the garnet are remnant gold coating. Ion microprobe pits are visible and are labeled in $\delta^{18}O$ (‰ VSMOW) with an uncertainty of ±0·5‰. Core, low-Z and high-Z annuli within the second resorption boundary have lower $\delta^{18}O$ than does the outermost mid-Z rim. Variability in the outer rim is greater than the uncertainty; however, all analyses with $\delta^{18}O$ <6·7‰ overlap the outermost ~5 µm rim. The analysis pit marked with 'X' overlaps an inclusion.

region (less distinct than the low-Z annulus of the JS eclogite sample), coupled with a 50–100 µm thick high-Z rim. A Mn X-ray map (Fig. 5b) shows slight enrichment in the core of the garnet with a relatively high-Mn rim coupled with faint radial zoning. A compositional traverse (C–C′, Fig. 5a and c) shows a core composition of ($Alm_{60}Grs_{26}Pyp_{10}Sps_4$) with gradually decreasing Fe and Mn and increasing Mg, coupled with constant Ca, moving rimward ($Alm_{58}Grs_{25}Pyp_{14}Sps_3$). Closer to the rim, Mn increases gradually whereas Ca remains stable, and Fe continues to decrease and Mg continues to increase ($Alm_{55}Grs_{24}Pyp_{16}Sps_6$). This outermost region of the garnet core has less well-defined margins than the zoning in the JS eclogite garnet, but is visible as the low-Z portions of Fig. 5a that have elevated Mn in Fig. 5b. Finally, the outermost garnet rim is characterized by an abrupt jump in Fe coupled with decrease in Ca ($Alm_{59}Grs_{19}Pyp_{16}Sps_6$), followed by a gradual increase in Ca and decrease in Fe towards the edge of the crystal ($Alm_{56}Grs_{23}Pyp_{16}Sps_6$), whereas Mn and Mg remain relatively constant. The thickness of the outer rim is highly variable given the resorbed nature of these garnets.

Three garnets (PNP-1, PNP-2 and PNP-3) from the Panoche Pass hornblendite were analyzed for their oxygen isotope composition and were also found to be zoned (Tables 1 and 2; Electronic Appendix 1). In traverse C–C′ (Fig. 5c), the garnet core from PNP-1 (including Mn-enriched edges of the core region) is homogeneous in $\delta^{18}O$ (11·1 ±0·3‰, $n = 7$). However, the isotopic composition of the outer rim is strikingly different, although similarly homogeneous (6·5 ± 0·4‰, $n = 5$). The other garnets measured were found to have a similar pattern, with the addition of distinct patches of intermediate $\delta^{18}O$ in the low-Z outer portions of the cores close to the rims. Figure 6 shows a high-contrast BSE image near the rim of garnet PNP-2. The core $\delta^{18}O$ in this garnet is similar to or slightly higher (11·3–11·7‰) than that of PNP-1 in Fig. 5c. The thin, high-Z outer rim of the garnet has a similarly low $\delta^{18}O$ (<6·8‰, constrained by a single analysis that overlaps with the core). In this traverse near the edge of the ~1 mm garnet, the gradient in $\delta^{18}O$ at the rim–core margin is constrained to 4·5‰ over 12 µm. Unlike garnet PNP-1 (Fig. 5), PNP-2 was found to contain faint ~100–200 µm diameter patches of intermediate $\delta^{18}O$ (8·9–9·5‰, Fig. 6). These intermediate $\delta^{18}O$ zones appear to be small domains (perhaps connected in the third dimension) and not additional concentric zoning. These patches ($Alm_{62}Grs_{25}Pyp_{12}Sps_1$) are compositionally similar to the surrounding garnet ($Alm_{62}Grs_{26}Pyp_{11}Sps_1$), and are only faintly visible in high-contrast BSE owing to a difference in average Z of ~0·1% (Fig. 6).

$\delta^{18}O$ of matrix minerals

The $\delta^{18}O$ of the whole-rock and selected matrix phases from the JS eclogite and PNP hornblendite were analyzed by laser fluorination on ~2 mg samples (Table 3; Fig. 7). Bulk samples of garnet from eclogite ($\delta^{18}O = 4·8 \pm 0·1$‰, 2 SD, $n = 4$) and hornblendite (10·0 ± 0·1‰, 2 SD, $n = 2$) do not reflect the significant isotopic heterogeneity apparent in the ion microprobe analyses, but have intermediate $\delta^{18}O$ between rim and core values as determined by ion microprobe. Bulk garnet $\delta^{18}O$ is closer to that of the cores, as would be expected for mixed analyses of small volumes of rim material with larger volumes of core material. Omphacite from the JS eclogite (5·8 ± 0·1‰, 2 SD, $n = 2$) and hornblende from the PNP hornblendite (6·1 ±0·1‰, 2 SD, $n = 2$) are substantially different from the coexisting garnet, the other major phase in these rocks. Given the small degree of fractionation between pyroxene and garnet, and hornblende and garnet, even at low temperatures (e.g. Kohn & Valley, 1998*a*, 1998*b*), these differences imply disequilibrium. Retrograde titanite has $\delta^{18}O = 5·3$‰ in the eclogite sample and 4·7‰ in the hornblendite sample. The $\delta^{18}O$ values of whole-rock powders are 6·3‰ (eclogite) and 7·2‰ (hornblendite). The combined mode of garnet and omphacite, or hornblende, is greater than 90% in these samples. Although the hornblendite whole-rock $\delta^{18}O$ value is a plausible combination of garnet and hornblende $\delta^{18}O$ values, the whole-rock $\delta^{18}O$ value of the eclogite sample is higher than those of garnet and omphacite, indicating the presence of some volumetrically minor, but significantly ^{18}O-enriched reservoir.

Texturally late quartz from the JS eclogite was analyzed for $\delta^{18}O$ by ion microprobe (Table 2; Electronic

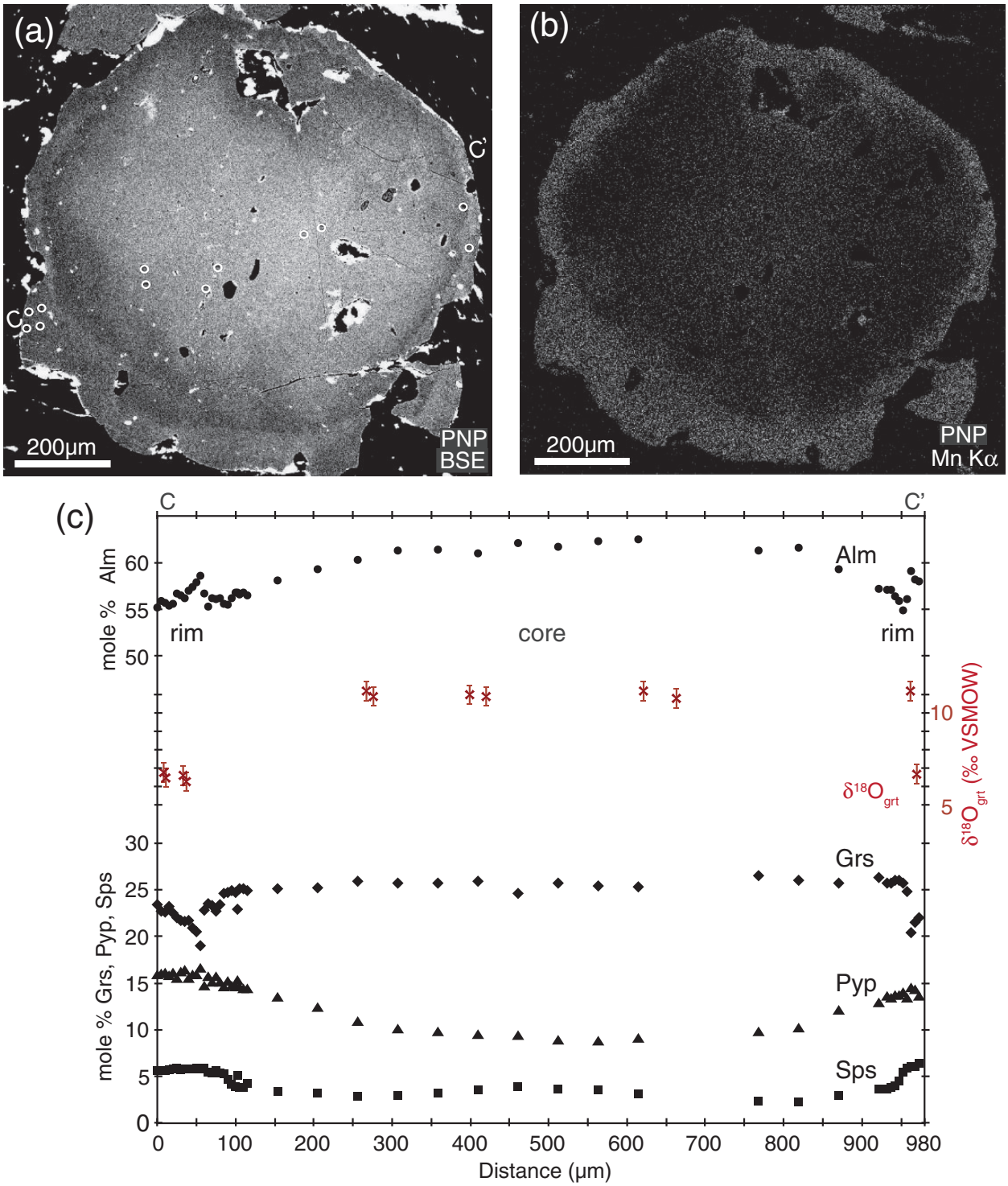

Fig. 5. Zoned garnet PNP-l from the Panoche Pass hornblendite. (a) High-contrast BSE image of the garnet with a patchy core and 50–100 μm high-Z rim. Ion microprobe pits used to measure $\delta^{18}O$ on the traverse C–C′ are shown as white circles. The black matrix and inclusions are hornblende; bright white patches are remnants of the gold coating used for ion microprobe analysis. (b) Mn Kα X-ray map of the same garnet showing slightly higher Mn concentration (bright) in the core decreasing towards the high-Mn rim. (c) Electron- and ion-microprobe traverse C–C′ shown in (a). Ion microprobe $\delta^{18}O$ data are shown as crosses. Analytical uncertainty is shown at the 2 SD level when larger than the data points.

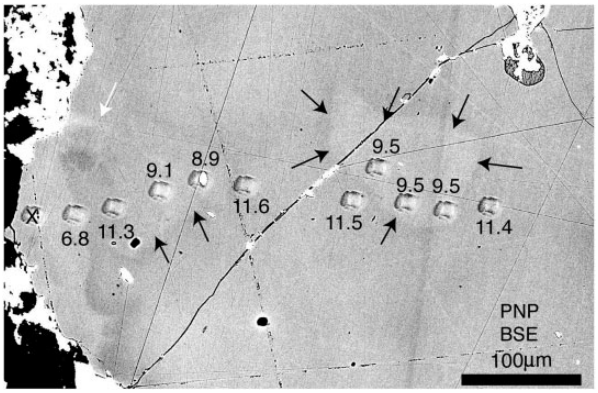

Fig. 6. High-contrast BSE image of the edge of garnet PNP-2 from the Panoche Pass hornblendite. Ion microprobe pits are labeled in $\delta^{18}O$ (‰ VSMOW) with an uncertainty of ±0·5‰. The outermost analysis pit (marked with 'X') is excluded because of a crack through the pit bottom. Bright white patches are remnant gold coating. Cation variability visible as average atomic number is faint and patchy with the exception of the contrast between the edge of the homogeneous low-Z, high-$\delta^{18}O$ core and high-Z, low-$\delta^{18}O$ rim. Patchy regions of intermediate $\delta^{18}O$ appear to correspond to zones of slightly higher Z and are indicated with black arrows. An apparently healed fracture extending into the core region of the garnet from the rim with similar BSE contrast to the intermediate $\delta^{18}O$ patches is indicated with a white arrow.

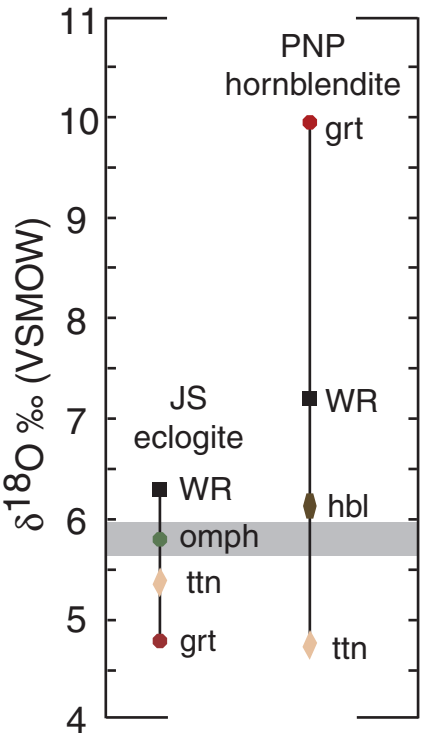

Fig. 7. Mineral and whole-rock (WR) $\delta^{18}O$ of the JS eclogite and PNP hornblendite by laser fluorination. The gray band represents the oxygen isotope composition of unaltered mid-ocean ridge basalts [$\delta^{18}O(WR) = 5{\cdot}6 \pm 0{\cdot}2$‰; Eiler, 2001]. It should be noted that the WR $\delta^{18}O$ of the JS eclogite cannot be explained as a sum of the $\delta^{18}O$ of major phases (see Fig. 8).

Table 3: Mineral and whole-rock $\delta^{18}O$ from the Junction School eclogite and Panoche Pass hornblendite by laser fluorination

	$\delta^{18}O$ (‰, VSMOW)		
Sample	Average	2 SD	*n*
JS eclogite			
garnet	4·8	0·1	4
omphacite	5·8	0·1	2
titanite	5·3		1
whole-rock	6·3		1
PNP hornblendite			
garnet	10·0	0·1	2
hornblende	6·1	0·1	2
titanite	4·7		1
whole-rock	7·2		1

Analyses corrected to UWG-2 = 5·80‰, VSMOW.

Appendix 1). Matrix quartz in the JS eclogite occurs along grain boundaries between garnet and omphacite (Figs 1c and 8). Polygonal crystals grade into micrometer-scale veins that appear to wet grain boundaries between zoned omphacite crystals. Texturally late quartz has uniformly high $\delta^{18}O$ (25·4 ± 0·2‰, 2 SD, $n = 4$, Fig. 8), providing an explanation for the high whole-rock values described above.

Zoned zircon

Junction School

Zircon in the Junction School eclogite occurs as inclusions in garnet, omphacite, epidote and titanite, as well as between grains of matrix phases. Inclusions within zircon grains are generally small (~1 µm) and are not identifiable in thin section, either because they were plucked during polishing, or because they are not mineral but fluid inclusions. Zircon found along the margins of matrix minerals, as inclusions in texturally late epidote, chlorite and titanite, or in the rims of omphacite or garnet (Fig. 1b and c) is typically euhedral. In Fig. 1b euhedral zircon is found in the outer acmite-rich rims of matrix omphacite, and in Fig. 1c an aggregate of small euhedral zircon grains is found within the blueschist-facies high-Z annulus in garnet. These zircon grains or aggregates are nearly featureless in BSE images and have a diffuse oscillatory zoning in CL. Rare, larger zircons separated from the Junction School eclogite are clear and subhedral, 150–200 µm in length, with poorly developed terminal pyramids. They contain inclusions of phengite,

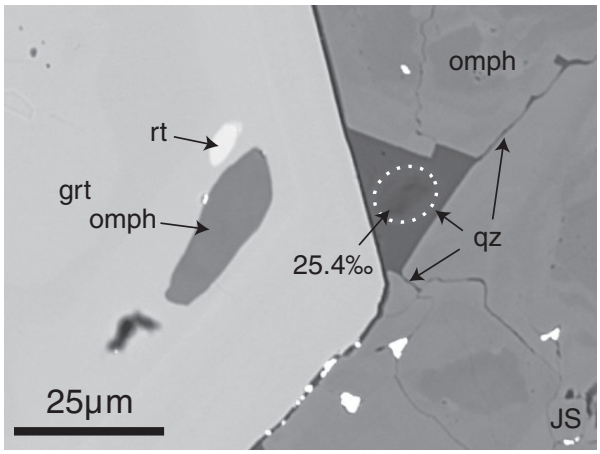

Fig. 8. Low-contrast BSE image of texturally late, polygonal quartz and associated veins adjacent to garnet and omphacite in JS eclogite. Bright spots are remnant gold coating or rutile. The ion microprobe analysis in quartz is outlined in white dots and yields a $\delta^{18}O$ of 25·4‰. The presence of a trace of high-$\delta^{18}O$ quartz explains the bias in $\delta^{18}O$(WR) values (Fig. 7).

omphacite, quartz, epidote, and chlorite. Zircons separated from the JS eclogite are similar in morphology, BSE, and CL characteristics to texturally late zircon observed in thin section, but are much larger. Separated zircons are relatively featureless in BSE images, but in CL images have distinct cores surrounded by fine-scale, but somewhat diffuse, oscillatory zoned rims (Fig. 9a–f). Many separated zircons appear to be fragments of longer crystals with chevron-shaped oscillatory CL zones appearing to grow in one direction (Fig. 9a–c). Zircon cores (when apparent) are featureless and dark (Fig. 9d), have faint, diffuse zoning (Fig. 9e) or are patchy (Fig. 9f).

The $\delta^{18}O$ values of zircons from the JS eclogite are bimodal and correlate with the zoning patterns identified in CL (Figs 9 and 10a). Ion microprobe $\delta^{18}O$ data are summarized in Table 2 with complete results presented in Electronic Appendix 3. Patchy CL cores are uniformly low in $\delta^{18}O$ (4·6 ± 0·6‰, $n = 5$). Oscillatory-zoned rims are substantially higher in $\delta^{18}O$ (6·4 ± 0·5‰, $n = 8$).

Selected zircons were also analyzed from the JS sample for trace elements by ion microprobe (Fig. 10a and b; Table 4). Zircon cores have higher REE (454–2590 ppm) and Y (615–4145 ppm) concentrations than zircon rims (68–110 ppm REE; 141–182 ppm Y). Zircon cores also have higher Th/U ratios (0·27–0·60) than oscillatory-zoned rims (0·01–0·03; Fig. 10a). On chondrite-normalized REE diagrams, zircon cores display a positive Ce anomaly (Ce/Ce* = 13–33) and a negative Eu anomaly (Eu/Eu* = 0·3–0·5, Fig. 10b). Zircon rims are more strongly depleted in LREE and middle REE (MREE), with virtually no Ce anomaly (Ce/Ce* = 0·7–2·4) and a small negative Eu anomaly (Eu/Eu* = 0·5–0·6). Both cores and rims have steep heavy REE (HREE) patterns.

JS zircons were also analyzed for U–Pb isotopes by ion microprobe (Table 5); ages were calculated and Tera–Wasserburg concordia diagrams (Fig. 10c) were constructed with Isoplot 3.0 (Ludwig, 2003). Analyses were not corrected for common lead, and lie on mixing lines between common lead (Mattinson, 1986) and the reported concordia intercept age. U–Pb isotopic analysis of zircon from the JS eclogite was made difficult by the low concentrations of U (rims 5–24 ppm; cores 11–68 ppm). Uranium and thorium concentrations measured during the geochronology session are similar to those measured during the trace element session (Tables 4 and 5), with the exception that one rim geochronology analysis yielded 55 ppm U and a Th/U ratio of 0·5. Unfortunately, this grain was plucked during sample preparation after U–Pb analysis and could not be analyzed further. With the exception of this grain, zircon rims analyzed for geochronology have an average U concentration of 9 ppm with Th/U = 0·01–0·03. Previous attempts to date Franciscan eclogite metamorphism by U–Pb on titanite (Mattinson, 1986) were also problematic because of the extremely low levels of U in that phase. Although chemically and texturally distinct, zircon cores and rims from the JS eclogite do not have a resolvable difference in age, with cores yielding a low-precision concordia intercept age of 141 ± 22 Ma ($n = 8$, MSWD = 2·4) and rims yielding 144 ± 10 Ma ($n = 9$, MSWD = 1·3).

Panoche Pass

Zircon in the Panoche Pass hornblendite occurs in thin section along grain boundaries at the rims of matrix minerals or along fractures (Fig. 1e and f). Zircon separated from the PNP hornblendite is clear, generally euhedral, and 150–200 µm in length, but with a slightly rounded appearance. It is substantially more abundant than that separated from the JS eclogite. CL images show oscillatory and sector zoning (Fig. 9g–j), but do not have the distinct core–rim textural differences visible in the JS zircons. In one case (Fig. 9i) a diffuse oscillatory-zoned rim appears to truncate more distinct zoning in the core region, implying a multi-stage growth history for this grain. Panoche Pass zircon has very few inclusions, although one large (~20 µm) titanite inclusion is present in one zircon. No zircons similar in size to the separated fraction have been observed in thin section.

The $\delta^{18}O$ values of zircons (Figs 9 and 10d) from the PNP hornblendite are summarized in Table 2 with the complete dataset presented in Electronic Appendix 3. In general, zircon $\delta^{18}O$ is higher (8·2 ± 1·1‰, $n = 22$) in the PNP sample than in the core or rim populations of the JS eclogite, although no systematic zoning pattern correlated with CL patterns was observed.

The trace element chemistry of selected zircons is reported in Table 4, with analysis locations indicated in Fig. 9. As with oxygen isotopes, trace element analyses

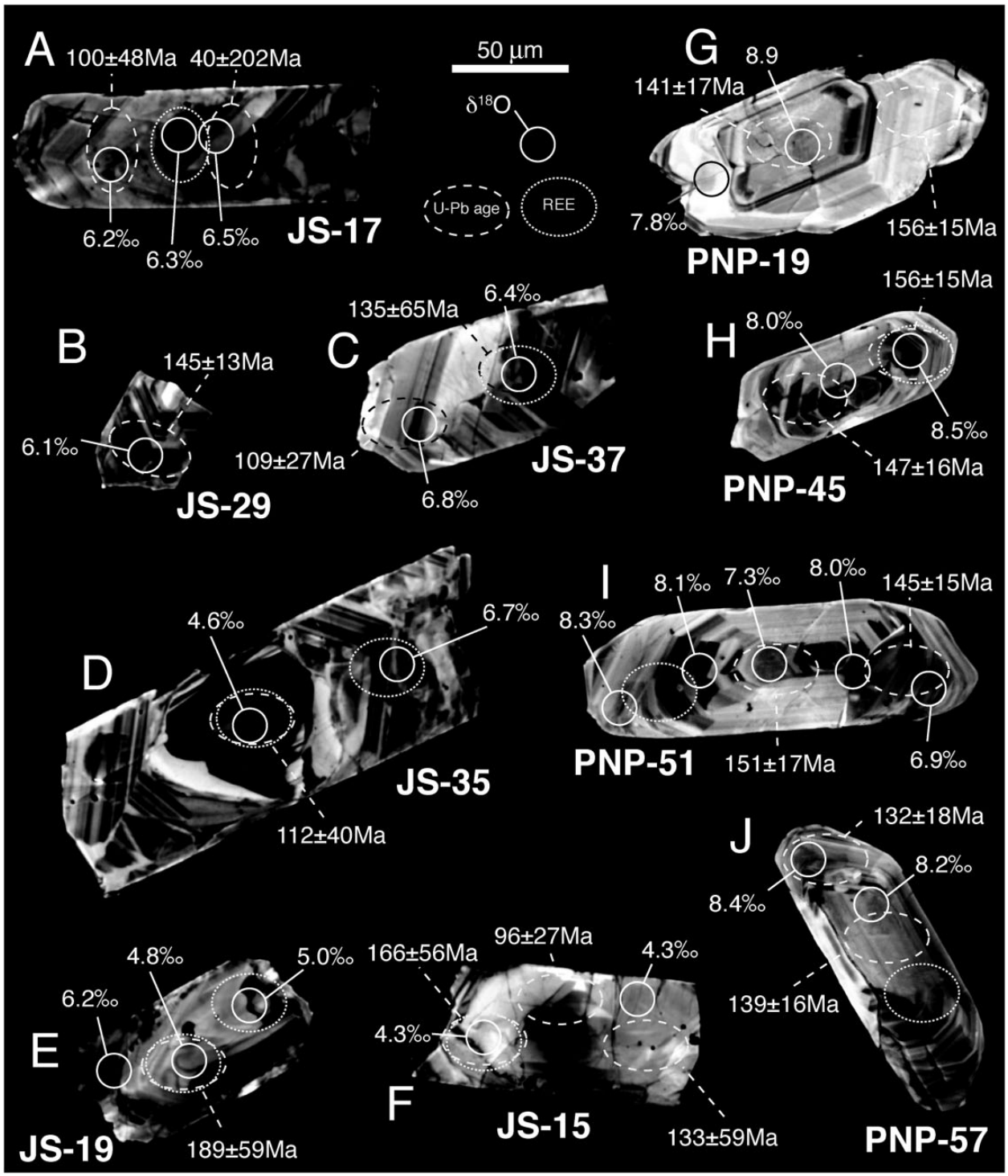

Fig. 9. Panchromatic cathodoluminescence (CL) images of zircons separated from the JS eclogite (a–f) and PNP hornblendite (g–j). The location and size of ion microprobe analysis pits for age are indicated by ellipses. Oxygen isotope analyses (continuous-line circles) are labeled with $\delta^{18}O$ (‰ VSMOW). U–Pb analyses (dashed) are labeled with ^{238}U–^{206}Pb spot ages. The locations of REE analyses are indicated by dotted ellipses. Some JS zircons (d–f) preserve oscillatory-zoned or dark-CL cores with distinctively low $\delta^{18}O$. PNP zircons display oscillatory and sector zoning without distinct cores.

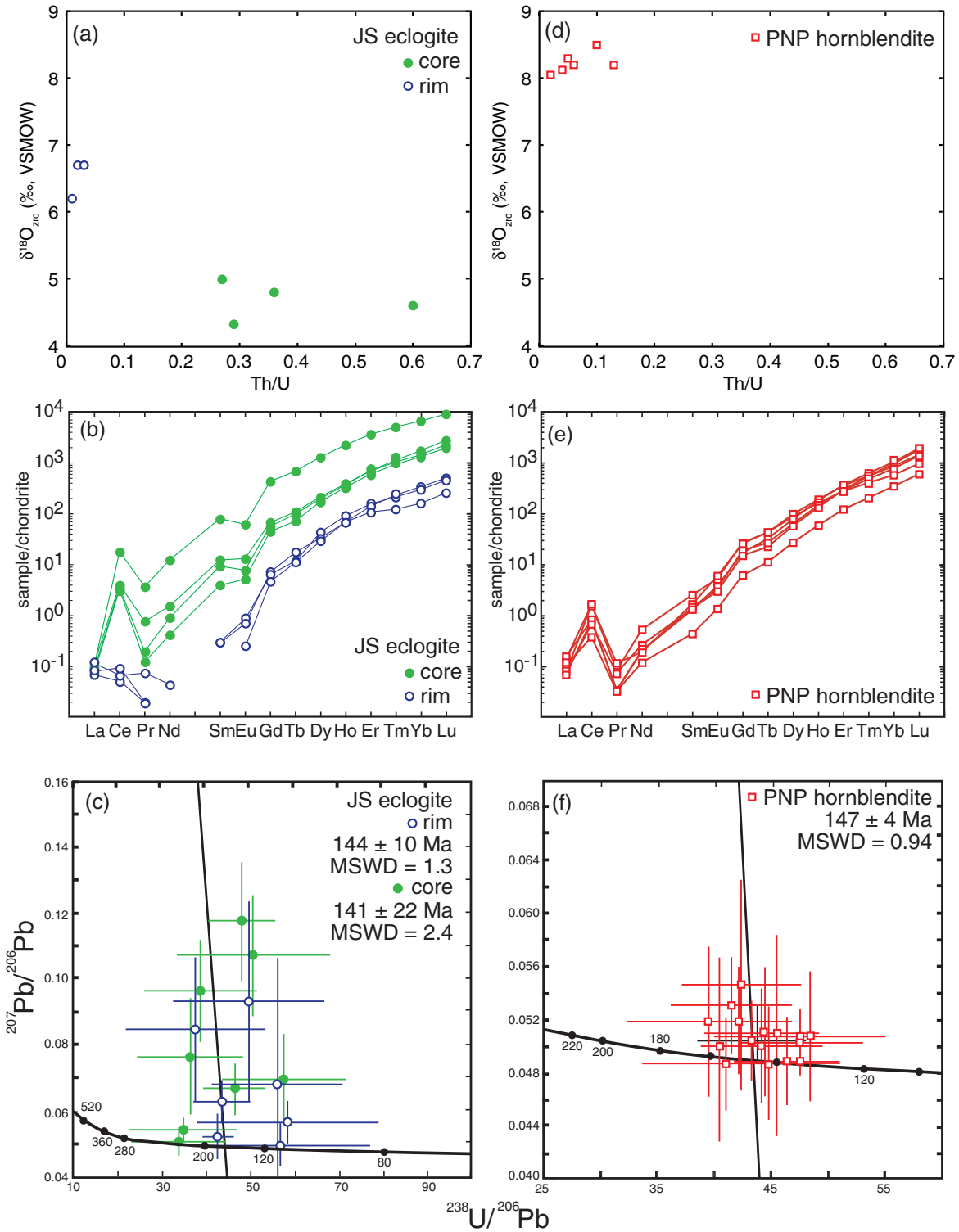

Fig. 10. Trace element, $\delta^{18}O$, and U–Pb isotope analyses of Franciscan zircon. Junction School eclogite zircon cores are represented by filled circles, rims by open circles. Panoche Pass hornblendite zircon data are plotted as open squares. (a) $\delta^{18}O$ vs Th/U of zircons from the Junction School eclogite (only samples with both classes of data analyzed are shown). (b) Chondrite-normalized REE diagram for zircons from the Junction School eclogite. JS eclogite zircon cores have a higher REE content than the rims, positive Ce and negative Eu anomalies. (c) Tera–Wasserburg concordia diagram for zircons from the Junction School eclogite. The regression line is shown for the rim analyses only. (d) $\delta^{18}O$ vs Th/U of Panoche Pass zircons in hornblendite. Elevated $\delta^{18}O$ and low Th/U ratios preclude an igneous origin at a mid-ocean ridge. (e) Chondrite-normalized REE diagram for zircons from the Panoche Pass hornblendite. (f) Tera–Wasserburg concordia diagram for zircons from the Panoche Pass hornblendite. Uncertainties are indicated at the 2σ level.

Table 4: Ion microprobe trace element analyses (ppm) of selected zircons from the JS eclogite and PNP hornblendite measured at WiscSIMS

Sample	La	Ce	Pr	Nd	Sm	Eu	Gd	Tb	Dy	Ho	Er	Tm	Yb	Lu	∑REE	Ti	Y	Hf	Th	U	Th/U
JS eclogite																					
z15-c*	0·02	1·92	0·01	0·18	0·57	0·28	8·68	2·55	41·5	18·2	95·6	22·4	215	47·2	454	13·9	615	8693	2	7	0·29
z17-r	0·02	0·03	n.d.	n.d.	0·05	0·05	1·28	0·43	10·8	5·2	25·4	5·27	49·6	11·4	110	1·8	182	12666	0	7	0·01
z19-c	0·02	2·07	0·02	0·40	1·35	0·43	10·96	3·51	47·6	20·5	111	27·1	282	67·2	574	5·5	721	9115	4	14	0·27
z19-c	0·03	2·39	0·07	0·68	1·79	0·73	12·95	3·91	51·5	21·3	109	25·2	232	55·2	517	4·8	749	9416	7	20	0·36
z35-c	0·03	10·79	0·32	5·49	11·72	3·43	84·3	24·7	315·1	124·2	577	123·2	1090	221	2590	6·4	4145	8540	91	152	0·60
z35-r	0·02	0·06	n.d.	n.d.	0·04	0·04	1·43	0·64	8·31	3·9	17·5	3·02	26·6	6·39	67·9	2·2	141	8974	0	8	0·02
z37-r	0·03	0·04	0·01	0·02	n.d.	0·01	0·93	0·41	7·18	3·9	22·9	5·81	56·4	12·6	110	7·3	145	12 027	0	4	0·03
PNP hornblendite																					
z23-1	0·02	0·23	n.d.	0·05	0·06	0·08	1·21	0·40	6·6	3·2	19·3	4·9	56·1	14·5	107	2·1	136	7344	2	89	0·02
z23-2	0·02	0·41	0·01	0·12	0·20	0·17	2·94	0·81	14·0	7·3	46·8	13·3	156	43·5	286	1·7	313	6955	2	40	0·04
z33	0·02	0·49	n.d.	0·09	0·21	0·19	3·71	0·97	15·4	8·0	45·2	11·6	125	33·4	244	3·2	315	7139	3	54	0·06
z45	0·03	0·99	0·01	0·24	0·37	0·30	5·29	1·55	23·8	10·5	56·8	13·2	140	34·9	288	4·5	402	6916	13	134	0·10
z51	0·02	0·97	0·01	0·09	0·24	0·33	5·11	1·56	21·2	9·0	44·0	9·8	93·6	23·3	209	4·2	331	7665	24	185	0·13
z57	0·04	0·50	n.d.	0·09	0·19	0·21	3·33	1·16	18·9	10·0	58·2	15·0	168	46·8	322	3·2	389	6833	3	63	0·05

n.d., not detected.
*c, core; r, rim.

reveal a relatively homogeneous composition, with Y (136–404 ppm) and REE (107–323 ppm) intermediate between the core and rim analyses of the JS eclogite. Th/U ratios range from 0·02 to 0·13 (Fig. 10d). On a chondrite-normalized REE diagram, zircons have a small positive Ce anomaly (Ce/Ce* = 6·5–17) and a negative Eu anomaly (Eu/Eu* = 0·7–0·9), and generally steep HREE (Fig. 10e).

Zircons from the Panoche Pass hornblendite were also analyzed for U–Pb isotopes by ion microprobe (Table 5, Fig. 10f). Th and U concentrations and Th/U ratios were consistent with those measured along with the other trace elements. The PNP hornblendite zircons have higher U concentration than those from the JS eclogite, and provided more precise results and concordant analyses with lower counting times, yielding an intercept age of 147 ± 4 Ma (MSWD = 0·94, n = 16).

DISCUSSION

Compositional and isotopic zoning in garnet and zircon have long been used to reconstruct pressure, temperature, fluid and time histories of metamorphic rocks. Zircon is a highly refractory mineral with slow intracrystalline diffusion of both cations (e.g. Hanchar & Hoskin, 2003; Cherniak, 2010) and oxygen (Valley *et al.*, 1994; Watson & Cherniak, 1997; Valley, 2003; Page *et al.*, 2007*c*; Bowman *et al.* 2011). Garnet is also an extremely robust mineral with sluggish diffusion rates for both oxygen and cations, particularly at the low temperatures (<600°C) recorded in these rocks (e.g. Coghlan, 1990; Vielzeuf *et al.*, 2005; Ganguly, 2010). The snapshot of geochemical conditions provided by these minerals during their crystallization is unlikely to be substantially modified, barring wholesale dissolution, particularly at the low temperatures found in subduction regimes. Indeed, the very heterogeneities observed in both cation and isotopic compositions are testimony to the ability of these minerals to preserve geochemical information. Correlation of $\delta^{18}O$ data and REE patterns allows a synthesis of records preserved in the zircon and garnet. U–Pb data from zircons allow this relative history to be placed in the context of absolute chronology and compared with other Franciscan tectonic blocks. Thermobarometry on inclusions in zoned garnets (where available) can be used to tie this record to the P–T path of these rocks, generating whole or partial P–T–t–fluid paths in a subduction tectonic setting.

Cation zoning in garnets

Junction School

Garnets from the JS eclogite record a rather complete record of prograde growth during subduction from early blueschist-facies conditions in the Mn-rich cores (10 kbar, 400°C) to the highest-grade eclogite-facies conditions (22 kbar, 550°C) recorded in the outer-core region just

Table 5: Ion microprobe U–Pb isotopic data from Junction School eclogite and Panoche Pass hornblendite zircons

	Isotopic ratios				Calculated ages							
	$^{206}Pb/^{238}U$	2σ	$^{207}Pb/^{235}U$	2σ	$^{206}Pb^*/^{238}U$	2σ	$^{207}Pb^*/^{235}U$	2σ	% $^{206}Pb^*$	U	Th	Th/U
JS eclogite												
z3-r	0·0182	0·0064	0·0962	0·193	116·0	40·4	93·3	179·0	91·59	7·8	0·1	0·01
z3-c	0·0166	0·0058	0·0696	0·048	106·2	37·0	68·3	45·4	96·77	24·8	9·1	0·37
z5-c	0·0209	0·0032	0·1123	0·062	133·2	20·2	108·1	57·0	96·56	25·5	9·9	0·39
z11-r	0·0157	0·0033	n.d.	n.d.	100·2	20·8	n.d.	n.d.	74·97	8·4	0·2	0·03
z15c1	0·0261	0·0089	0·1264	0·256	165·8	56·0	120·9	230·0	94·97	11·1	3·6	0·32
z15c1	0·0208	0·0077	n.d.	n.d.	132·9	48·8	n.d.	n.d.	80·41	11·1	7·6	0·68
z19-c	0·0290	0·0094	0·1201	0·077	184·4	58·6	115·1	69·8	97·44	47·1	32·1	0·68
z23-r	0·0220	0·0032	0·0772	0·086	140·0	20·4	75·5	80·8	95·42	24·3	0·8	0·03
z25-c	0·0221	0·0034	0·1270	0·029	140·9	21·6	121·4	26·0	98·63	78·1	46·4	0·59
z29-r	0·0227	0·0021	0·0783	0·074	144·8	13·4	76·5	70·0	96·66	55·2	27·7	0·50
z29-c	0·0266	0·0094	n.d.	n.d.	169·5	59·2	n.d.	n.d.	92·35	48·6	20·2	0·42
z35-c	0·0176	0·0063	0·1030	0·049	112·1	40·0	99·5	45·0	99·13	66·7	39·0	0·59
z37-r	0·0212	0·0103	n.d.	n.d.	135·4	64·8	n.d.	n.d.	79·62	4·6	0·1	0·03
z37-r	0·0171	0·0047	0·0790	0·166	109·4	29·6	77·2	155·8	95·68	7·5	0·0	0·01
PNP hornblendite												
z1-1	0·0226	0·0028	0·1535	0·023	144·3	17·3	145·0	19·9	99·89	177·6	17·6	0·10
z1-2	0·0210	0·0024	0·1428	0·015	134·0	15·3	135·6	13·3	99·88	240·6	32·8	0·14
z3-1	0·0239	0·0031	0·1540	0·032	152·1	19·3	145·5	28·0	99·20	95·2	4·7	0·05
z3-2	0·0212	0·0029	0·1628	0·042	135·0	18·5	153·2	36·6	97·52	127·0	17·6	0·14
z5	0·0250	0·0033	0·1215	0·018	159·2	21·0	116·5	16·3	99·86	265	8·6	0·03
z7	0·0253	0·0045	0·1811	0·036	161·1	28·4	169·0	30·8	100·00	95·9	9·1	0·09
z11	0·0406	0·0396	0·2897	0·284	256·4	246	258·3	224·0	99·76	97	18·3	0·19
z19	0·0222	0·0028	0·1304	0·027	141·3	17·7	124·4	24·0	99·23	117·5	7·2	0·06
z25	0·0222	0·0023	0·1263	0·039	141·6	14·6	120·7	35·6	98·76	81·2	9·3	0·11
z27	0·0243	0·0044	0·1496	0·031	154·5	27·4	141·6	27·8	99·51	192·1	24·6	0·13
z31	0·0404	0·0372	0·0676	0·131	255·0	230	66·4	124·4	95·1	75	11·2	0·15
z45-1	0·0230	0·0025	0·1546	0·019	146·8	16·0	145·9	16·6	99·78	117·8	13·4	0·11
z45-2	0·0245	0·0024	0·1432	0·042	156·0	15·2	135·9	37·2	99·06	48·5	4·4	0·09
z47-1	0·0231	0·0029	0·1197	0·050	147·1	18·3	114·8	45·8	97·85	51·9	4·6	0·09
z49	0·0213	0·0021	0·1166	0·021	136·0	13·6	112·0	19·5	98·85	67	12·9	0·19
z51-1	0·0228	0·0024	0·1558	0·019	145·3	15·2	147·0	16·7	99·81	197·7	14·9	0·08
z51-2	0·0237	0·0026	0·1621	0·023	150·7	16·7	152·6	20·2	99·72	94·3	7·0	0·07
z57-1	0·0207	0·0029	0·1447	0·023	131·8	18·3	137·2	20·6	100·00	90·1	7·7	0·09
z57-2	0·0219	0·0026	0·1364	0·033	139·3	16·2	129·9	29·6	99·30	51·7	5·4	0·10

n.d., not detected.

inside the high-Mn, low-Z annulus (Page *et al.*, 2007*a*). This prograde growth zonation is truncated by an irregular boundary followed by a sharp compositional shift of elevated Mn and depleted Fe (Figs 2 and 3). This increase in Mn is both outside the resorption boundary and very sharp, unlike the commonly observed (in higher grade rocks) upward turn seen inside the resorption boundary characteristic of Mn back-diffusion into the garnet during dissolution.

There are several possibilities for the origin of Mn enrichment in this annulus. The source of Mn could be locally derived from previously resorbed garnet or another Mn-bearing phase that was liberated during the lacuna in garnet growth and scavenged by the neoformed garnet.

Alternatively, the Mn could have been introduced into the rock by an external fluid during garnet resorption or at the beginning of new garnet growth. The sharp rise at the resorption boundary and prolonged elevation in Mn content of this annulus may be evidence for an external source of Mn. Annuli of compatible elements in garnet that have been interpreted as having formed in a closed system typically have a sharp peak in Mn followed by a smooth decrease in Mn consistent with a Rayleigh model of compatible element fractionation (e.g. Yang & Rivers, 2003). The plateau in spessartine content visible in the low-Z annulus (Fig. 3) and the oscillating behavior in the outermost rim are not consistent with a simple dissolution–regrowth history, despite the presence of resorption boundaries inside the Mn annuli. The Mn source may have been in part the resorbed garnet, but some substantial, fluid-mediated redistribution of Mn is the most likely cause of these Mn annuli. The low-Mn, high-Z annulus located between both Mn-enriched annuli contains a blueschist-facies mineral assemblage (Page *et al.*, 2007*a*), requiring that rim development occurred after substantial exhumation.

Oscillatory-zoned garnets were first reported from Franciscan eclogites by Dudley (1969), from the Tiburon peninsula. Their presence there was recently reconfirmed by the optical observations of Tsujimori *et al.* (2006*a*). Although zoning patterns in eclogite garnet have been described as a kinetic phenomenon (Ghent, 1988), more recently, oscillatory zonation in garnets from mélange-hosted eclogite has been interpreted to record inflections in the exhumation P–T path (García-Casco *et al.*, 2002; Blanco-Quintero *et al.*, 2011). The zoning described by García-Casco *et al.* (2002) is similar to that seen here. However, that reported by Blanco-Quintero *et al.* (2011) is much broader than that observed in the other studies described above, with zones as wide as 500 μm in a 5 mm garnet. One possible origin for the >10 μm-scale zoning in the JS eclogite is a similar series of inflections in the P–T path. However, extremely fine-scale zoning found exclusively in the rims of eclogite garnets (Dudley, 1969; García-Casco *et al.*, 2002; Tsujimori *et al.*, 2006*a*) is more likely to preserve a record of changing fluid conditions during exhumation, similar to the record preserved in hydrothermal skarn garnets (e.g. Jamtveit *et al.*, 1993; Jamtveit & Hervig, 1994; Clechenko & Valley, 2003; Page *et al.*, 2010; D'Errico *et al.*, 2012).

Panoche Pass

Cation zoning in the PNP hornblendite garnet is much more diffuse than that found in the JS eclogite. The core regions of garnet preserve relatively subdued prograde zonation with increasing Mg and decreasing Fe, suggestive of growth under increasing T. There is no existing detailed P–T work on inclusions in this garnet, which are limited to hornblende, quartz, ilmenite and apatite. The faint zones of Mn enrichment inward from the rim (Fig. 5c) suggest recrystallization along cracks or perhaps dissolution–recrystallization phenomena, leaving a somewhat 'ghost-like' high-Z core with the diffuse margins visible in Fig. 5a. The broad and relatively homogeneous Mn-rich rim is not consistent with diffusion of Mn into the garnet during resorption because of its flat-topped morphology in compositional traverse (Fig. 5c). If it were the product of regrowth from a fixed reservoir after resorption, an asymmetrical peak would be expected, followed by depletion of Mn owing to its removal from the matrix. The homogeneity of the Mn contents in the rim suggests growth with a continual supply of Mn, either at the expense of a dissolving Mn-rich phase (perhaps ilmenite) or from an external fluid. The sudden increase in Fe with concomitant decrease in Ca at the outer rim may be due to a fluid change—for example, by entrainment in a reducing environment such as a serpentinite, or owing to renewed crystallization at a different P and T.

Oxygen isotopes

The oxygen isotope results for all mineral and whole-rock analyses (with the exception of quartz in the JS eclogite; Table 2) are within the range commonly observed for eclogites and related rocks (e.g. Putlitz *et al.* 2000; Russell, 2011; Russell *et al.* 2013, and references therein). The JS eclogite and PNP hornblendite are basaltic in composition, and are generally believed to have a mid-ocean ridge basalt (MORB) protolith (Hermes, 1973; Sorensen *et al.*, 1997). Unaltered gabbros from ophiolites and unaltered MORB record a consistent whole-rock $\delta^{18}O$ of 5·6‰, whereas basalts that experienced low-T alteration with seawater are enriched in ^{18}O ($\delta^{18}O_{WR} = 5{\cdot}6$–$14$‰) and gabbros that interacted with water at high T take on lower values of $\delta^{18}O$ (2–5·6‰; see Eiler, 2001, for a review). Previous rock- and mineral-scale studies have demonstrated that many eclogites and related rocks preserve this seafloor alteration signal through high-P metamorphism and exhumation (e.g. Putlitz *et al.*, 2000, 2001; Früh-Green *et al.*, 2001; Fu *et al.*, 2010; Halama *et al.*, 2011; Russell *et al.*, 2013).

Disequilibrium among minerals

A first-order question in the interpretation of the oxygen isotope record of these rocks is an assessment of equilibrium and the scale of exchange between the minerals. Even at the low metamorphic temperatures (<600°C) typical of Franciscan high-grade blocks, equilibrium fractionation between the major phases in these feldspar-absent mafic lithologies is small. The fractionation between omphacite and almandine-rich garnet [$\Delta^{18}O$ (omph–grt)] was found to be 0·02–0·46‰ for 600–650°C alpine eclogites (Kohn & Valley, 1998*b*). Larger fractionations [$\Delta^{18}O$ (omph–grt) = 0·72‰ at 500°C] were found among

the lower T eclogites of Syros, Greece (Putlitz *et al.*, 2000). Fractionation between the core and rim values of the JS eclogite garnet and bulk analyzed omphacite yield $\Delta^{18}O$ (omph–grt core) = 1·8‰, and $\Delta^{18}O$ (omph–grt rim) = −0·2‰. The garnet cores are clearly out of equilibrium with the bulk omphacite. Although the fractionation between garnet rims and bulk omphacite could be consistent with high-T equilibrium, given the results of Kohn & Valley (1998*b*), a late high-T event is not recorded in Franciscan blocks and suggests oxygen isotope disequilibrium between garnet rims and matrix omphacite as well. Matrix omphacite in this rock is strongly zoned in cations, and may preserve a heterogeneous $\delta^{18}O$ record to complement that preserved by the garnets. Texturally late titanite ($\delta^{18}O$ = 5·3‰; Table 3) similarly must be in disequilibrium with all garnet core and rim values at the T recorded by the inclusions (Valley *et al.*, 2003; Page *et al.*, 2007*a*). Finally, the extremely elevated $\delta^{18}O$ void-filling quartz (25‰) would require T < 100°C to be in equilibrium with any other phase measured in the rock, and is probably a late, fluid-precipitated phase (Valley *et al.*, 2003). The high $\delta^{18}O$ value of the quartz is consistent with low-temperature (~200°C) equilibrium with vein calcite ($\delta^{18}O$ ~20‰) found within Franciscan host sediments (Sadofsky & Bebout, 2001).

Measured $\delta^{18}O$ of the phases present in the PNP hornblendite similarly reveals profound disequilibrium. The fractionation of oxygen isotopes between hornblende and almandine-rich garnet is negligible at any reasonable temperature (Kohn & Valley, 1998*a*). Therefore, garnet cores are in extreme disequilibrium with bulk matrix hornblende [$\Delta^{18}O$ (hbl–grt core) < −5‰], whereas the thin, low-$\delta^{18}O$ rims could be in equilibrium with the matrix hornblende [$\Delta^{18}O$ (hbl–grt rim) = −0·3‰]. Texturally late matrix titanite may also be in equilibrium with garnet rims, with $\Delta^{18}O$ (sph–grt rim) = −1·7‰ yielding T ~500 ± 80°C, or might be in disequilibrium if they were formed at lower temperatures (Valley *et al.*, 2003).

The mineral-scale disequilibrium found in these two samples is consistent with recent results from high-grade blocks throughout the Franciscan (Pincus *et al.*, 2010; Errico *et al.*, 2013). The evidence for late fluid exchange, extreme heterogeneity and disequilibrium recorded in these Franciscan metamorphic rocks stands in contrast to the apparently pristine ocean-floor alteration record preserved in most eclogites (e.g. Putlitz *et al.*, 2000, 2001; Früh-Green *et al.*, 2001; Halama *et al.*, 2011).

Garnet zoning

Although $\delta^{18}O$ zoning in garnet has been recognized in skarn garnets (e.g. D'Errico *et al.*, 2012), and in an ultra-high-pressure metasediments (Sobolev *et al.*, 2011), such zoning in almandine-rich garnets in pelitic and mafic lithologies is reported rarely in the literature, and then is generally <1‰ (Kohn *et al.*, 1993; Skelton *et al.*, 2002; Martin *et al.*, 2006; Lancaster *et al.*, 2009). One notable exception to this is the ~4‰ zoning reported in garnets from migmatites in the Pyrenees (Vielzeuf *et al.*, 2005). A recent study of eclogite garnets from nine European localities has revealed the presence of up to 2·5‰ zoning with lower $\delta^{18}O$ cores and higher $\delta^{18}O$ rims, suggesting a late prograde fluid interaction with a higher $\delta^{18}O$, more mantle-like, reservoir (Russell *et al.*, 2013). The ~3‰ zoning observed in the JS garnets and the ~5‰ zoning observed in the PNP garnets are thus rather dramatic for metamafic rocks. Recently, Errico *et al.* (2013) have documented similar ~3‰ zoning in other Franciscan eclogite garnets. Because of the low temperatures recorded in these samples (<600°C) and the slow intracrystalline diffusion of oxygen in garnet, the zoning represents a primary record of crystallization (or, locally, recrystallization; e.g. Martin *et al.*, 2011*a*; Raimondo *et al.*, 2012) conditions as opposed to diffusional resetting.

Ion microprobe oxygen isotope analyses of garnets from the JS eclogite yield a bimodal distribution with low-$\delta^{18}O$ cores and high-$\delta^{18}O$ rims (Fig. 11a). The low-$\delta^{18}O$ (~4‰) portions of the garnets include the garnet cores, as defined by cation zonation, the low-Z annulus, and the blueschist-facies high-Z annulus (Figs 2 and 4), which have broadly homogeneous $\delta^{18}O$. Only the outermost garnet rims, outside a second resorption boundary, have elevated $\delta^{18}O$ (6–7‰, Fig. 4).

The JS garnet core $\delta^{18}O$ of 4·3‰ is low for the range of garnet values recorded in eclogite, and is consistent with that recorded in metagabbros that have experienced higher-temperature hydrothermal alteration at a mid-ocean ridge. Feldspar-free metamorphic lithologies such as those in this study are characterized by relative homogeneity of $\delta^{18}O$ between phases because of the small fractionation between the limited number of minerals that make up the rock (Kohn & Valley, 1998*a*, 1998*b*). In general, the $\delta^{18}O$ of eclogitic garnet is typically less than 0·5‰ lower than the equilibrium whole-rock composition even at T < 600°C (e.g. Putlitz *et al.*, 2000). Most JS garnet core analyses are more than 0·5‰ lower in $\delta^{18}O$ than the range of unaltered MORB whole-rocks (Fig. 11a), suggesting that the MORB protolith of the JS eclogite was altered by seawater at medium to high temperatures, similar to ophiolitic gabbros (Eiler, 2001). Because of the absence of a significant high-$\delta^{18}O$ mineral reservoir in this eclogite, the only plausible explanation for the extreme (2–3‰) shift in $\delta^{18}O$ at the garnet rim is the influx of an externally derived, high-$\delta^{18}O$ fluid.

Panoche Pass hornblendite garnets preserve three $\delta^{18}O$ domains (Fig. 11b). The $\delta^{18}O$ values of garnet cores are 10·9–11·7‰, recrystallized patches are 8–9‰, and the outermost high-Z rims yield uniformly low ratios (6·2–6·8‰). Negligible oxygen isotope fractionation between hornblende and almandine garnet allows direct

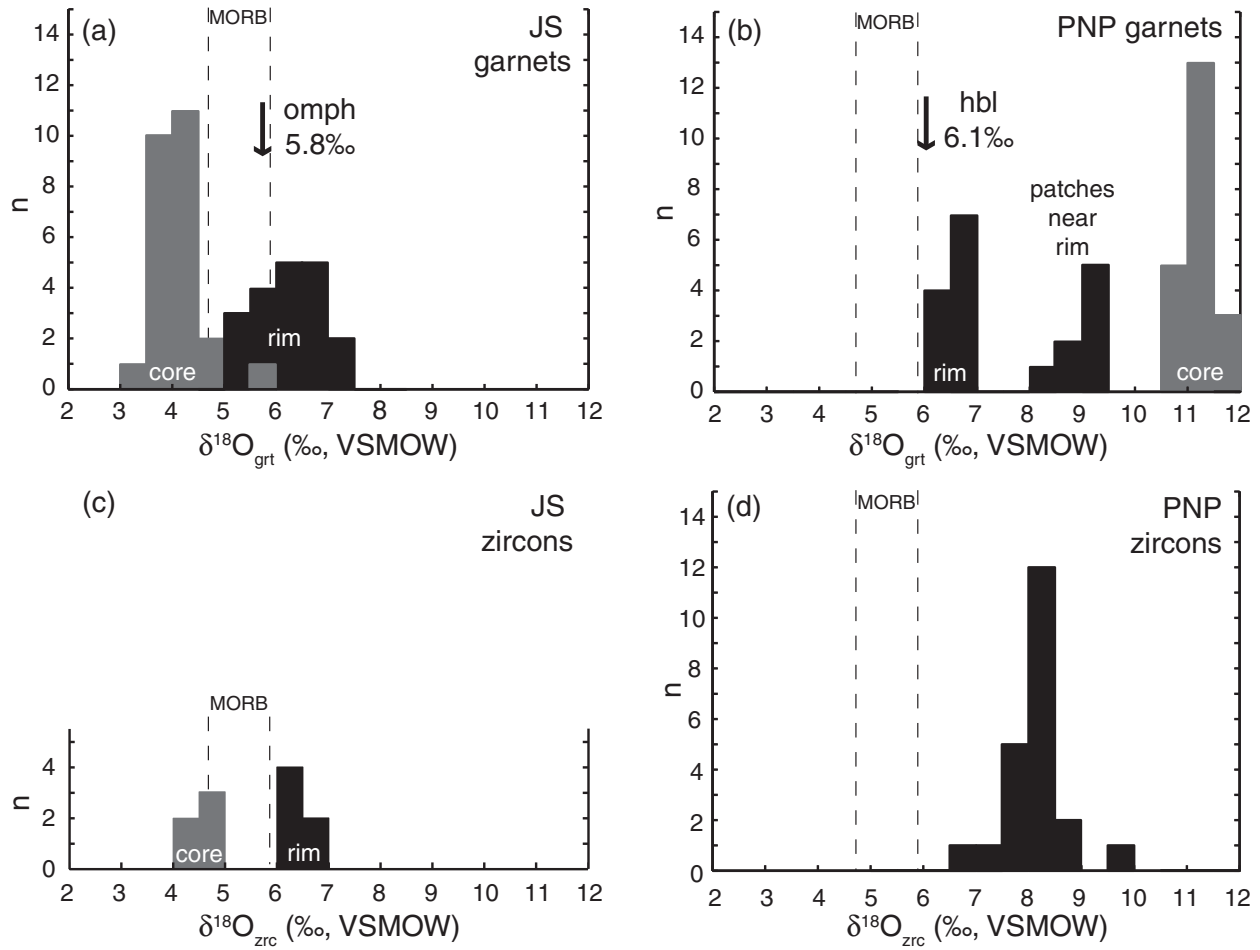

Fig. 11. $\delta^{18}O$ values of garnet (a, b) and zircon (c, d) by ion microprobe. Core regions shown in gray; all other textures shown in black. The dashed lines indicate the range of primitive mantle values of $\delta^{18}O$ (zrc) = 5·3 ± 0·6‰ (Valley *et al.*, 1998; Page *et al.*, 2007*b*). The fractionation between zircon and almandine garnet is smaller than the analytical uncertainty for all reasonable temperatures [$\Delta^{18}O$ (zrc–grt) <0·2‰ for T > 300°C; Valley *et al.*, 2003], and so garnet and zircon $\delta^{18}O$ values can be directly compared. The dominant matrix phase $\delta^{18}O$ measured by laser fluorination is indicated by black arrows in (a) and (b).

comparison among these minerals and equilibrium whole-rock compositions. The elevated ^{18}O of PNP garnet cores is well above the value of unaltered MORB (Fig. 11b), requiring that a MORB protolith be altered at low temperatures on the ocean floor, prior to metamorphism. The outermost low-$\delta^{18}O$ rim is in equilibrium with matrix hornblende, and records the influx of a less ^{18}O-enriched fluid. Given the slow rate of intracrystalline oxygen diffusion in garnet and textural evidence of resorption, both before and after rim formation, the intermediate $\delta^{18}O$ patches are best explained as zones of recrystallization, perhaps along healed fractures. Although texturally less distinct than the evidence of zoning and resorption recorded in the JS garnets, these intermediate $\delta^{18}O$ domains are likewise best explained by resorption and regrowth of garnet in a changing $\delta^{18}O$ fluid environment. These patches may have formed in a dissolution–reprecipitation process similar to that documented by Martin *et al.* (2011*a*).

Zircon zoning

Zircon from the JS eclogite preserves a bimodal distribution of oxygen isotope ratios (Fig. 11c), similar to those found in the garnets of the same rock. The distinctive core–rim CL textures present in JS zircons are, in some ways, similar to magmatic zircons with metamorphic rims. However, a magmatic origin at a mid-ocean ridge is not consistent with the oxygen isotope ratios (4·6‰) found in the cores of JS zircons. Igneous zircons occurring in oceanic gabbros display a distinctively narrow range of $\delta^{18}O$ (5·2 ± 0·5‰; Cavosie *et al.*, 2009; Grimes *et al.*, 2011), characteristic of their formation from a mantle reservoir. The oxygen isotope record of zircons from the ocean-floor environment is robust: igneous zircon from the ocean floor can even retain a mantle signature through metasomatic conversion of its host-rock to jadeitite in a subduction environment (Fu *et al.*, 2010). Although some $\delta^{18}O$ values

from JS zircon cores overlap the mantle range, most are not consistent with a mantle origin for the JS zircon cores, as would be expected for igneous zircons from MORB.

The oxygen isotope fractionation between zircon and almandine-rich garnet is negligible, allowing the zircon and garnet record to be directly compared (Valley *et al.*, 1994, 2003). All JS zircon core $\delta^{18}O$ values overlap with the core compositions of coexisting garnets (Fig. 11a and c), suggesting that they formed from the same oxygen reservoir as garnets: altered oceanic crust. Zircon rims ($\delta^{18}O = 6{\cdot}4‰$) from the JS eclogite are more enriched in ^{18}O than the cores, similar to values found in garnet rims (6·4‰; Fig. 11a and c). Because they have the same $\delta^{18}O$, zircon rims are in equilibrium with garnet rims, but may also have formed any time after the influx of the high-$\delta^{18}O$ fluid responsible for the isotopic zoning in garnet.

The oxygen isotope ratios of zircons from the PNP hornblendite record a different history. The 8·2‰ $\delta^{18}O$ value of these zircons precludes an igneous origin in equilibrium with the mantle, despite the MORB-like composition of the whole-rock. Similarly, a metamorphic origin in equilibrium with high-$\delta^{18}O$ garnet cores (11·3‰) or low-$\delta^{18}O$ garnet rims (6·6‰) is also ruled out (Fig. 11b and d). The zircon oxygen isotope ratios overlap substantially with intermediate $\delta^{18}O$ value recrystallized zones in garnet (Fig. 11b and d), suggesting that they formed in a similar fluid environment.

Zircon textures, geochronology and trace elements

Texturally, the Junction School eclogite and Panoche Pass hornblendite zircon grains show diffuse oscillatory zoning in CL, features that in other rocks have been attributed to an igneous origin. Despite a superficial similarity to igneous zircon, a number of lines of evidence argue against this conclusion. The formation of oscillatory-zoned zircon is not exclusive to igneous environments, but is also found in zircons formed in high-pressure hydrothermal veins. Liati & Gebauer (1999) and Rubatto *et al.* (1999) reported metamorphic ages for eclogites based on euhedral, oscillatory-zoned zircon from deformed quartz veins in the Rhodope zone of northern Greece and the Sesia–Lanzo zone of the western Alps, respectively. Rubatto & Hermann (2003) found similar textures in zircon from a vein in eclogites from Monviso in the western Alps. In the case of the JS and PNP zircons, oscillatory zoning is confined to high-$\delta^{18}O$ zircon that crystallized during or after high-pressure fluid metasomatism, and not in equilibrium with primitive mantle-derived magmas at a spreading center.

High-pressure, zircon-bearing vein material contains significant amounts of both rutile and zircon, suggesting that metamorphic fluids at eclogite-facies *P–T* have the ability to transport Zr and Ti over at least short distances. The formation of vein zircon and the movement of Zr and Ti in aqueous fluids suggest a high fluid/rock ratio over a prolonged period (Nadeau *et al.*, 1993; Philippot, 1993). Alternatively, $NaAlSi_3O_8$-bearing fluids dramatically increase rutile solubility, and probably also play a role in HFSE mobility in subduction systems (Antignano & Manning, 2008). Alkaline fluids such as those formed during serpentinization also increase Zr solubility and have been shown to result in neoformed zircon in serpentine-hosted eclogite (Rubatto *et al.*, 2008; Martin *et al.*, 2011*b*), rodingite (Li *et al.*, 2010), and jadeitite (e.g. Tsujimori *et al.*, 2006*b*; Mori *et al.*, 2011). Fu *et al.* (2010) found evidence of both igneous zircons with mantle-like $\delta^{18}O$ and low-$\delta^{18}O$ hydrothermal zircons in jadeitites from Japan.

The ages of zircon from both Franciscan samples are further suggestive of a metamorphic origin. The low-precision ages for JS eclogite zircon cores (141 ± 22 Ma) and rims (144 ± 10 Ma) are indistinguishable from one another, and the more precise PNP hornblendite zircon age (147 ± 4 Ma). These ages match the youngest metamorphic ages found in Franciscan blocks, typically associated with garnet blueschist- or blueschist-facies overprinting (Wakabayashi & Dimitru, 2007, and references therein), and are incompatible with an igneous origin.

Although there is no published geochronology for the JS eclogite, the PNP hornblendite has been the subject of several chronological studies that place the new zircon ages in context. Ross & Sharp (1988) performed some of the first $^{40}Ar/^{39}Ar$ geochronology in the Franciscan on a garnet hornblendite from Panoche Pass. They interpreted a 162 ± 2 Ma plateau as the hornblende cooling age, and attributed the total gas age of ~145 Ma (identical to the zircon age in this study) to late white mica intergrown with the hornblende. Anczkiewicz *et al.* (2004) produced a Lu–Hf age of 168·7 ± 0·8 Ma for this block, similar to, but slightly older than the hornblende age. The younger hornblende age is probably compromised by the later metasomatism, as any fluid pulse that shifts the bulk $\delta^{18}O$ by ~5‰ would probably at least partially reset the Ar geochronometer. However, it seems unlikely that the hornblende age dates the last stage of fluid metasomatism, as the higher $\delta^{18}O$ zircons post-date the hornblende age.

In addition to CL textures, oxygen isotopes, and arguments based on geochronology, trace-element chemistry is commonly used as a discriminant between igneous and metamorphic zircon (e.g. Rubatto, 2002). A canonical interpretation of the Th/U systematics of these Franciscan zircons would be that the high Th/U values of the JS zircon cores (Fig. 10a) record an igneous origin. The low U and Th concentration and the generally low Th/U ratios (0·01–0·13) of JS zircon rims and PNP zircons (Fig. 10a and d) are generally interpreted as evidence for a metamorphic origin. However, although Th/U ratios are commonly higher in igneous zircons than in metamorphic

zircon, this signature is by no means unequivocal. Metamorphic zircon can preserve elevated Th/U through growth in a closed system, recrystallization of magmatic zircon, or by growth at the expense of a high-Th/U phase (Möller & Kennedy, 2006). Because the preponderance of CL, oxygen isotope, and geochronological evidence points to a metamorphic origin for all Franciscan zircons in this study, our preferred interpretation is that the JS zircon cores are also metamorphic, despite the lack of universally low Th/U ratios.

REE patterns are perhaps the most commonly used tool to relate zircon ages to metamorphic events recorded in the matrix mineralogy, particularly in tracing zircon that has grown during or after the growth of garnet (e.g. Rubatto, 2002; Kelly & Harley, 2005; Lancaster *et al.*, 2009). The compatibility of the HREE in garnet reduces the availability of these elements during zircon growth, and results in a characteristic flat or negatively sloped HREE pattern on chondrite-normalized diagrams, despite the increasing compatibility (with increasing atomic number) of these elements in zircon (Rubatto, 2002). However, despite the abundance of garnet in the rocks in this study, all zircons analyzed have the steep HREE pattern found in zircons from garnet-free lithologies (Fig. 10b and e). A conventional interpretation of these data in garnet-bearing rocks would be that zircons formed before the onset of garnet crystallization. However, the oxygen isotope and geochronological data presented above are similarly incompatible with such an interpretation for all zircons except the JS cores, which may have grown before JS garnet but from the same oxygen reservoir.

Zircons with steep REE patterns may have grown late in the history of both rocks, during periods of garnet resorption, and possibly with an external source of REE. Alternatively, zircon with a steep HREE pattern may have formed simultaneously with garnet containing even higher concentrations of HREE. REE data from both garnet and zircon are required to fully address these possibilities, but are beyond the scope of the current study.

The JS eclogite zircon cores are likely to have grown after ocean-floor metasomatism (judging from the preserved low $\delta^{18}O$ values) during the early stages of metamorphism, before the onset of garnet growth (yielding a steep HREE pattern). Both the JS eclogite and PNP hornblendite garnets display textural evidence of resorption before a shift in $\delta^{18}O$. The oxygen isotope ratios of JS rim zircons overlap with those preserved in garnet rims, and PNP zircon $\delta^{18}O$ values match the intermediate recrystallized garnet values (Fig. 11). Depending on the HREE composition of the garnet with similar $\delta^{18}O$ values, these zircons may have grown during garnet resorption, or during or after the formation of neoformed garnet with similar oxygen isotope ratios.

Oscillatory-zoned high-$\delta^{18}O$ zircon from Franciscan samples is also notable for the small size of positive Ce anomalies in chondrite-normalized REE patterns (Fig. 10b and e). Trail *et al.* (2011, 2012) recently developed an experimentally calibrated oxybarometer to allow estimates of f_{O_2} based on the magnitude of the Ce anomaly in zircon and temperature. The combination of a small Ce anomaly and low temperatures of metamorphism characteristic of the Franciscan yield extremely reducing estimates based on the current calibration of the oxybarometer. Even with a temperature estimate as high as 600°C (the highest recorded by the JS eclogite; Page *et al.*, 2007*a*), the resulting calculated oxygen fugacities are below the iron–wüstite buffer for JS zircon rims and PNP zircons. Uncertainties in the low concentrations of LREE and extrapolation of experimental results to low temperatures are probably responsible for the unreasonable magnitude of this result. However, extremely reducing, alkaline fluids generated by serpentinization are a possible candidate for metasomatism and Zr mobility in subduction zones (e.g. Johnson & Harlow, 1999; Tsujimori *et al.*, 2005; Evans, 2010). Hydrothermal zircon in metasomatic jadeitite (Tsujimori *et al.*, 2006*b*; Fu *et al.*, 2010; Yui *et al.*, 2010, 2012; Mori *et al.*, 2011) and metasomatized ultramafic rocks (Dubinska *et al.*, 2004; Li *et al.*, 2010) is perhaps more analogous to Franciscan zircons than zircon in orogenic eclogite. Hydrothermal zircons (discriminated by Th/U and $\delta^{18}O$) from jadeitite (Mori *et al.*, 2011) and serpentinite (Tsujimori *et al.*, 2006*b*; Fu *et al.*, 2010) have similarly small Ce anomalies that would result in similarly low oxygen fugacity based on the Trail *et al.* (2012) calibration. Although these results suggest that the Trail *et al.* (2012) calibration does not extend to extremely low-T, low-f_{O_2} conditions, late zircon growth in the JS and PNP samples may have been formed by an influx of low-f_{O_2} serpentinite-derived, reducing fluids, perhaps the same fluids that caused garnet dissolution.

Fluid history and *P–T–t–*fluid paths

Taken together, the data described above present a series of metamorphic and fluid events recorded in two different high-grade tectonic blocks within the Franciscan Complex. Federico *et al.* (2007) have shown that adjacent eclogite and blueschist blocks in a serpentinite mélange in the western Alps can have diachronous P–T histories, and indeed different P–T paths, consistent with the tectonic models of Gerya *et al.* (2002). New chronological and geochemical data for these complex, polymetamorphic rocks are best evaluated in terms of P–T–t–fluid paths, as each block probably represents a different path through the subduction zone at differing times. The pooled paths can be used to discuss the subduction zone evolution as a whole, rather than directly comparing ages and geochemical traces of fluid between blocks with an assumed common history.

Although the widespread oxygen isotope disequilibrium between the major phases in these rocks might initially cause dismay, it records a wealth of now interpretable data. Integration of oxygen isotope and trace element data measured using an *in situ* technique on garnet and zircon allows for the development of a robust fluid and tectonic history for each sample that can be presented in the form of a *P–T–t*–fluid path (Fig. 12), or, in the case of the PNP hornblendite where there is no robust *P–T* information, a fluid–time path (Fig. 13).

The igneous protolith of the Junction School eclogite was probably a mid-ocean ridge gabbro that was altered by high-temperature, sub-solidus, hydrothermal interaction. High-temperature fluids shifted the protolith $\delta^{18}O$ (whole-rock) to <5‰ before subduction ($\delta^{18}O$ is preserved in zircon and garnet cores formed after the beginning of metamorphism). The low-precision age of the metamorphic zircon cores (141 ±22 Ma) is consistent with other Franciscan eclogite ages of 150–160 Ma (Wakabayashi & Dumitru, 2007). The *P–T* record of the subduction path begins with blueschist-facies garnet cores with no evidence of subduction-related fluid metasomatism from an external source, through the peak of eclogite-facies metamorphism over 70 km deep beneath the Franciscan trench (22 kbar, Fig. 12). The garnet record was truncated by resorption at or after the peak of metamorphism, and then begins again after substantial exhumation to 30–50 km depth. The $\delta^{18}O$ of the eclogite garnet remained constant through this first stage of exhumation, with no evidence of exchange with external fluids. If this initial resorption episode was the result of changing fluid conditions reducing the stability of garnet, these fluids were apparently equilibrated with the eclogite and left no lasting mark on the oxygen isotope record of this rock. After another, less-pronounced period of resorption, new garnet growth began, this time with elevated $\delta^{18}O$ (Fig. 12). This metasomatism is approximately dated at 144 ± 10 Ma by high-$\delta^{18}O$ zircon. The *P–T* conditions of the elevated-$\delta^{18}O$ garnet and zircon rims are not constrained, but the temperature is unlikely to be substantially lower than for the blueschist-facies garnet, given the already low temperatures of ~400°C. Finally, late hydrothermal fluids precipitated high-$\delta^{18}O$ quartz along grain boundaries in a separate, and probably much later event, perhaps during the final stages of exhumation and emplacement in a sedimentary mélange at low temperatures.

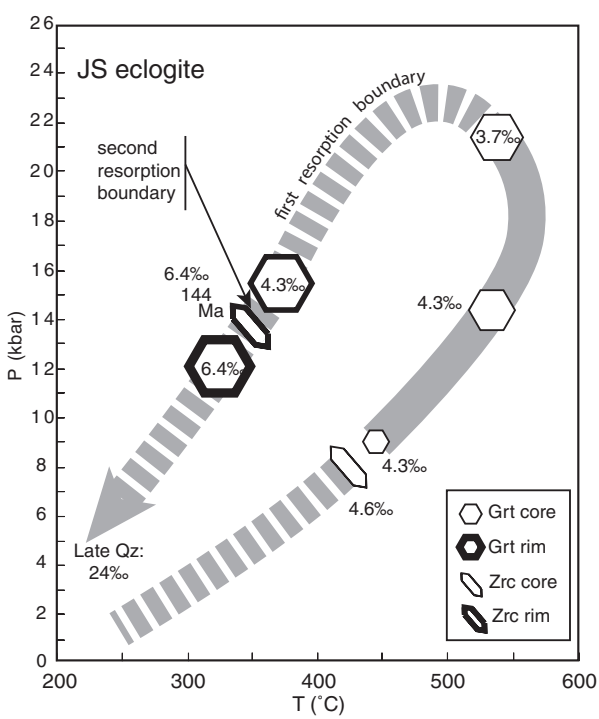

Fig. 12. *P–T–t*–fluid path for the Junction School eclogite. *P–T* loop is modified from Page *et al.* (2007*a*), and is dashed where inferred. $\delta^{18}O$ of garnet is indicated with hexagons and $\delta^{18}O$ and age information from zircon is indicated with zircon-shaped symbols. This path records early metamorphic zircon formation and prograde garnet with $\delta^{18}O$ values inherited from the altered ocean crust protolith. After garnet resorption, neoformed garnet records a similar oxygen isotope environment after substantial exhumation. Rims of zircon and garnet record a late fluid event.

It is unclear why garnet in the JS eclogite stopped growing after the highest *P* recorded by the inclusions in garnet, was resorbed, then began to grow again at blueschist-facies conditions. One possibility is that the rock moved out of the garnet stability field because of a change in bulk composition, such as metasomatism by an oxidizing fluid stabilizing epidote in favor of garnet (e.g. Donohue & Essene, 2000). Another possibility is that garnet was resorbed after exhumation of the eclogite block and re-equilibration below the pressures required to form garnet, then reburied to blueschist-facies conditions. This process has been described in the Alps by Rubatto *et al.* (2011) as 'yo-yo subduction', and has also been recorded in zoned garnet in mélange-hosted eclogite (Blanco-Quintero *et al.*, 2011). The broad-scale cation zoning in the JS eclogite bounded by resorption boundaries could be a result of changing *P* conditions and convection in the subduction channel, and the finer-scale oscillations in outermost garnet rims may represent a changing fluid record, similar to a skarn garnet, superimposed on the tectonic zoning. Following this line of reasoning, and given the two resorption boundaries present in these garnets, the arrow in Fig. 12 might be redrawn as a series of loops with *P–T* conditions returning to somewhere near the origin during the two periods of garnet resorption, and representing three burial–exhumation events in the same subduction channel. Recent work on serpentinites in the Franciscan has also uncovered evidence of 2–3 cycles of subduction–exhumation (e.g. Wakabayashi, 2012). Yo-yo subduction provides a plausible mechanism for the ubiquitous blueschist-facies overprint found in Franciscan blocks (e.g. Essene & Fyfe, 1967;

Moore & Blake, 1989), as well as an alternative model for the counter-clockwise subduction *P–T* path first proposed by Wakabayashi (1990).

Whether or not the eclogite block was on its way back to the surface following the exhumation path shown in Fig. 12, or if it was undergoing repeated reburial beneath the Franciscan trench, at the time of metasomatism, the JS block was no longer part of a coherent subducting slab, but was already a block within the mélange of the subduction channel (e.g. Cloos, 1986; Bebout, 2007). A fundamental difference in this oxygen isotope zonation and that described by Russell *et al.* (2013) is that the metasomatism in this case happened after the peak of metamorphism and after substantial exhumation. Although the high $\delta^{18}O$ rules out a fluid in equilibrium with a mantle reservoir (e.g. Putlitz *et al.*, 2000), the metasomatizing fluid in this channel could have been in equilibrium with serpentinized ultramafic rocks, sedimentary matrix, or both. The serpentinite body adjacent to the JS eclogite was recently found to have an elevated $\delta^{18}O$ (whole-rock) value of 7·9‰ (Barnes *et al.*, 2013). Other work on Franciscan serpentinite blocks has suggested that they, like the garnet-bearing blocks in this study, were similarly metasomatized by a high-$\delta^{18}O$ fluid (King *et al.*, 2003). Given the degree of metasomatism in the JS eclogite block, and the requisite high fluid/rock ratios needed to generate this shift in $\delta^{18}O$, the most likely cause is the high volume of fluids probably flowing up the subduction channel, originating from devolatilization of the subducting slab (e.g. Bebout, 2007). The zoning observed in the JS eclogite differs from that observed by Errico *et al.* (2013) in three other Franciscan eclogites, all of which had lower $\delta^{18}O$ rims than cores, explained by residence in low-$\delta^{18}O$ serpentinites. One possible explanation of this discrepancy is local differences in permeability and fluid–rock buffering within the subduction channel.

Like the Junction School eclogite, the Panoche Pass hornblendite has a basaltic composition probably formed at a mid-ocean ridge. Evidence of low-temperature hydrothermal alteration of the basalt is preserved in the elevated $\delta^{18}O$ (~11‰) of garnet cores (Fig. 13) that began to grow at ~169 Ma (Anczkiewicz *et al.*, 2004). Garnet rims (~6‰) are in oxygen isotope equilibrium with matrix hornblende (~6‰) that formed at 162 ± 2 Ma (Ar–Ar; Ross & Sharp, 1988). This suggests that garnet growth, resorption, and rim growth occurred in the first 7 Myr after the beginning of garnet growth, recording a 4–5‰ shift in $\delta^{18}O$ (Fig. 13). This rapid metasomatism after the peak of metamorphism is followed by another fluid episode that increases rock $\delta^{18}O$ between 162 and 147 Ma. Zircon growth at 147 ± 4 Ma probably dates this event, synchronous with limited garnet recrystallization, although the $\delta^{18}O$ of the block may have already shifted prior to zircon growth. The decrease and subsequent increase in oxygen isotope ratios in this block records changing fluid environments in the subduction channel, either during exhumation or possibly during multiple exhumation–reburial cycles.

Taken together, the zoned garnets from these two distinct blocks in the Franciscan preserve a consistent story of hydrothermal events at an oceanic spreading center that are preserved through subduction metamorphism. Most of the garnet in these rocks records an unchanging $\delta^{18}O$, suggesting limited fluid interaction from external sources during prograde metamorphism and garnet growth while these rocks were part of the subducting slab. Garnet rims and texturally late zones of recrystallization record profound shifts in $\delta^{18}O$ consistent with metasomatism at high fluid/rock ratios during exhumation or during exhumation–reburial cycles. However, if cation zoning and resorption in the JS eclogite garnets are a result of exhumation and reburial in the subduction channel, constant $\delta^{18}O$ across the first resorption boundary is suggestive of limited fluid flow through the block even when hosted by mélange (e.g. Ague, 2007). Perhaps the JS eclogite block was larger (or less permeable) during its first reburial, and mechanical changes to the block allowed for high-$\delta^{18}O$ fluid infiltration during a second reburial. If this form of cryptic metasomatism is widespread

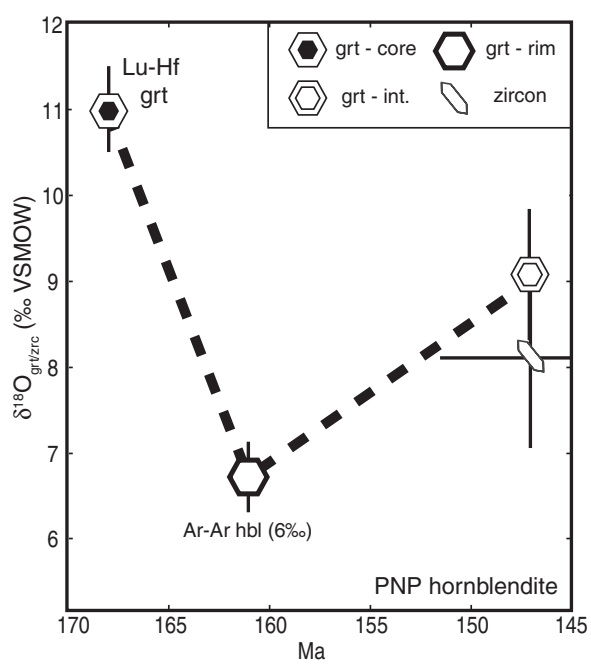

Fig. 13. Time–$\delta^{18}O$(fluid) path for the Panoche Pass hornblendite. Garnet growth begins at 169 Ma (Anczkiewicz *et al.*, 2004). Metasomatism at high fluid/rock ratios took place after garnet core growth and resorption, and was concluded by 162 Ma (garnet rims in equilibrium with 162 Ma hornblende; Ross & Sharp, 1988). Zircon growth occurred in a later fluid event, simultaneously with limited garnet recrystallization and late phengite growth (Ross & Sharp, 1988). Grt-int. indicates patches of intermediate $\delta^{18}O$ garnet. Uncertainty is shown at the 2 SD level when larger than the data points.

throughout the Franciscan (and beyond), then a vast unexploited record of subduction zone fluid history is available, provided that the metamorphic rocks that preserve it are closely scrutinized at the sub-grain mineral scale or smaller.

ACKNOWLEDGEMENTS

L. J. Sandler is thanked for assistance in field work. S. Passelaqua and J. Polidora generously allowed access to the Junction School locality. B. Hess, J. Kern, and P. Munk assisted in sample preparation. The authors are grateful to C. E. Henderson and J. Fournelle for assistance with the electron microprobe analyses; to M. Grove and C. W. Carrigan for help with U–Pb analyses; and to M. Spicuzza and N. T. Kita for assistance with oxygen isotope analyses. Comments by J. Barnes, T. Raimondo, an anonymous reviewer, and editor J. Hermann greatly improved this contribution.

FUNDING

This work was supported by the National Science Foundation (NSF) (grant EAR 00-87448) to S.B.M. and E.J.E. and (grant EAR 05-09639) to J.W.V., by a Sigma Xi Grant-in-aid and by the Turner Fund of the Department of Geological Sciences at the University of Michigan to F.Z.P. The electron microprobe and electron microscopes used in this work were funded by the NSF (grants EAR 96-28196, EAR 99-11352, CCLI 00-87895). WiscSIMS is partly supported by the NSF (grants EAR 03-19230, 07-44079, 10-53466) and the US Department of Energy (grant 93ER14389).

SUPPLEMENTARY DATA

Supplementary data for this paper are available at *Journal of Petrology* online.

REFERENCES

Ague, J. J. (2007). Models of permeability contrasts in subduction zone melange: Implications for gradients in fluid fluxes, Syros and Tinos Islands, Greece. *Chemical Geology* **239**, 217–227.

Anczkiewicz, R., Platt, J. P., Thirlwall, M. F. & Wakabayashi, J. (2004). Franciscan subduction off to a slow start: evidence from high-precision Lu–Hf garnet ages on high-grade blocks. *Earth and Planetary Science Letters* **225**, 147–161.

Antignano, A. & Manning, C. E. (2008). Rutile solubility in H_2O, H_2O–SiO_2, and H_2O–$NaAlSi_3O_8$ fluids at 0·7–2·0 GPa and 700–1000°C: Implications for mobility of nominally insoluble elements. *Chemical Geology* **255**, 283–293.

Bailey, E. H., Irwin, W. P. & Jones, D. L. (1964). *Franciscan and related rocks and their significance in the geology of western California. California Division of Mines and Geology Bulletin* **176.**

Barnes, J. D., Eldam, R., Lee, C.-T. A., Errico, J. C., Loewy, S. & Cisneros, M. (2013). Petrogenesis of serpentinites from the Franciscan Complex, western California, USA. *Lithos*, doi:10.1016/j.lithos.2012.12.018.

Barnicoat, A. & Cartwright, I. (1995). Focused fluid flow during subduction: oxygen isotope data from high-pressure ophiolites of the western Alps. *Earth and Planetary Science Letters* **132**, 53–61.

Bebout, G. E. (2007). Metamorphic chemical geodynamics of subduction zones. *Earth and Planetary Science Letters* **260**, 373–393.

Bebout, G. E. & Barton, M. D. (1989). Fluid flow and metasomatism in a subduction zone hydrothermal system: Catalina schist terrane, California. *Geology* **17**, 976–980.

Bebout, G. E. & Barton, M. (1993). Metasomatism during subduction: products and possible paths in the Catalina Schist, California. *Chemical Geology* **108**, 61–92.

Bebout, G. E. & Barton, M. D. (2002). Tectonic and metasomatic mixing in a high-*T*, subduction-zone melange: insights into the geochemical evolution of the slab–mantle interface. *Chemical Geology* **187**, 79–106.

Blanco-Quintero, I., García-Casco, A. & Gerya, T. V. (2011). Tectonic blocks in serpentinite mélange (eastern Cuba) reveal large-scale convective flow of the subduction channel. *Geology* **39**, 79–82.

Borg, I. Y. (1956). Glaucophane schists and eclogites near Healdsburg, California. *Geological Society of America Bulletin* **67**, 1563–1583.

Bowman, J. R., Moser, D. E., Valley, J. W., Wooden, J. L., Kita, N.T. & Mazdab, F. (2011). Zircon U–Pb isotope, $\delta^{18}O$ and trace element response to 80 M.y. of high temperature formation. *American Journal of Science* **311**, 719–772.

Breeding, C., Ague, J. & Bröcker, M. (2004). Fluid–metasedimentary rock interactions in subduction-zone melange: Implications for the chemical composition of arc magmas. *Geology* **32**, 1041–1044.

Catlos, E. J. & Sorensen, S. S. (2003). Phengite-based chronology of K- and Ba-rich fluid flow in two paleosubduction zones. *Science* **299**, 92–95.

Cavosie, A. J., Valley, J. W., Wilde, S. A. & EIMF (2006). Correlated microanalysis of zircon: Trace element, $\delta^{18}O$, and U–Th–Pb isotopic constraints on the igneous origin of complex >3900 Ma detrital grains. *Geochimica et Cosmochimica Acta* **70**, 5601–5616.

Cavosie, A. J., Kita, N. T. & Valley, J. W. (2009). Primitive oxygen-isotope ratio recorded in magmatic zircon from the Mid-Atlantic Ridge. *American Mineralogist* **94**, 926–934.

Cherniak, D. J. (2010). Diffusion in accessory minerals: zircon, titanite, apatite, monazite and xenotime. In: Zhang, Y. & Cherniak, D. J. (eds) *Diffusion in Minerals and Melts. Mineralogical Society of America and Geochemical Society, Reviews in Mineralogy and Geochemistry* **72**, 827–869.

Clechenko, C. C. & Valley, J. W. (2003). Oscillatory zoning in garnet from the Willsboro wollastonite skarn, Adirondack Mts, New York: a record of shallow hydrothermal processes preserved in a granulite facies terrane. *Journal of Metamorphic Geology* **21**, 771–784.

Cloos, M. (1986). Blueschists in the Franciscan Complex of California: petrotectonic constraints on uplift mechanisms. In: Evans, B. W. & Brown, E. H. (eds) *Blueschists and Eclogites. Geological Society of America, Memoir* **164**, 77–93.

Coghlan, R. A. N. (1990). Studies in diffusional transport: Grain boundary transport of oxygen in feldspars, diffusion of oxygen, strontium, and the REEs in garnet, and the thermal histories of granitic intrusions in south–central Maine using oxygen isotopes. PhD thesis, Brown University, Providence, RI.

Coleman, R. G. (1980). Tectonic inclusions in serpentinites. *Archives des Sciences* **33**, 89–102.

D'Errico, M. E., Lackey, J. S., Surpless, B. E., Loewy, S. L., Wooden, J. L., Barnes, J. D., Strickland, A. & Valley, J. W. (2012). A detailed record of shallow hydrothermal fluid flow in the Sierra Nevada magmatic arc from low-$\delta^{18}O$ skarn garnets. *Geology* **40**, 763–766.

Donohue, C. L. & Essene, E. J. (2000). An oxygen barometer with the assemblage garnet–epidote. *Earth and Planetary Science Letters* **181**, 459–472.

Donovan, J. J., Kremser, D. & Fournelle, J. H. (2009). Probe for Window's User's Guide and Reference, v.8.24, Enterprise Edition, 355 pp.

Dubinska, E., Bylina, P., Kozlowski, A., Dorr, W., Nejbert, K., Schastok, J. & Kulicki, C. (2004). U–Pb dating of serpentinization: hydrothermal zircon from a metasomatic rodingite shell (Sudetic ophiolite, SW Poland). *Chemical Geology* **203**, 183–203.

Dudley, P. P. (1969). Electron microprobe analyses of garnet in glaucophane schists and associated eclogites. *American Mineralogist* **54**, 1139–1150.

Eiler, J. (2001). Oxygen isotope variations of basaltic lavas and upper mantle rocks. In: Valley, J. W. & Cole, D. R. (eds) *Stable Isotope Geochemistry. Mineralogical Society of America and Geochemical Society, Reviews in Mineralogy and Geochemistry* **43**, 319–364.

Errico, J. C., Barnes, J. D., Strickland, A. & Valley, J. W. (2013). Oxygen isotope zoning in garnets from Franciscan eclogite blocks: evidence for rock-buffered fluid. *Contributions to Mineralogy and Petrology* **166**, 1161–1176, doi:10.1007/s00410-013-0915-0.

Essene, E. J. & Fyfe, W. S. (1967). Omphacite in Californian metamorphic rocks. *Contributions to Mineralogy and Petrology* **15**, 1–23.

Evans, B. (2010). Lizardite versus antigorite serpentinite: magnetite, hydrogen, and life (?). *Geology* **38**, 879–882.

Federico, L., Crispini, L., Scambelluri, M. & Capponi, G. (2007). Ophiolite mélange zone records exhumation in a fossil subduction channel. *Geology* **35**, 499–502.

Früh-Green, G., Scambelluri, M. & Vallis, F. (2001). OH isotope ratios of high pressure ultramafic rocks: implications for fluid sources and mobility in the subducted hydrous mantle. *Contributions to Mineralogy and Petrology* **141**, 145–159.

Fu, B., Valley, J. W., Kita, N. T., Spicuzza, M. J., Paton, C., Tsujimori, T., Bröcker, M. & Harlow, G. E. (2010). Multiple origins of zircons in jadeitite. *Contributions to Mineralogy and Petrology* **159**, 769–780.

Ganguly, J. (2010). Cation diffusion kinetics in aluminosilicate garnets and geological applications. In: Zhang, Y. & Cherniak, D. J. (eds) *Diffusion in Minerals and Melts. Mineralogical Society of America and Geochemical Society, Reviews in Mineralogy and Geochemistry* **72**, 559–601.

Ganor, J., Matthews, A., Schliestedt, M. & Garfunkel, Z. (1996). Oxygen isotopic heterogeneities of metamorphic rocks: an original tectonostratigraphic signature, or an imprint of exotic fluids? A case study of Sifnos and Tinos islands (Greece). *European Journal of Mineralogy* **8**, 719–732.

García-Casco, A., Torres-Roldan, R. L., Millan, G., Monie, P. & Schneider, J. (2002). Oscillatory zoning in eclogitic garnet and amphibole, Northern Serpentinite Melange, Cuba: a record of tectonic instability during subduction? *Journal of Metamorphic Geology* **20**, 581–598.

Gerya, T. V., Stöckhert, B. & Perchuk, A. L. (2002). Exhumation of high-pressure metamorphic rocks in a subduction channel: A numerical simulation. *Tectonics* **21**, 1056.

Getty, S. R. & Selverstone, J. (1994). Stable isotopic and trace-element evidence for restricted fluid migration in 2 GPa eclogites. *Journal of Metamorphic Geology* **12**, 747–760.

Ghent, E. D. (1988). A review of chemical zoning in eclogite garnets. In: Smith, D. C. (ed.) *Eclogites and Eclogite-facies Rocks. Developments in Petrology* **12**, 207–236.

Grimes, C. B., Ushikubo, T., John, B. E. & Valley, J. W. (2011). Uniformly mantle-like $\delta^{18}O$ in zircons from oceanic plagiogranites and gabbros. *Contributions to Mineralogy and Petrology* **161**, 13–33.

Halama, R., John, T., Herms, P., Hauff, F. & Schenk, V. (2011). A stable (Li, O) and radiogenic (Sr, Nd) isotope perspective on metasomatic processes in a subducting slab. *Chemical Geology* **281**, 151–166.

Hanchar, J. M. & Hoskin, P. W. O. (eds) (2003). *Zircon. Mineralogical Society of America and Geochemical Society, Reviews in Mineralogy and Geochemistry* **53**.

Harlow, G. E., Sisson, V. B., Ave Lallemant, H. G., Sorensen, S. S. & Seitz, R. (2003). High-pressure, metasomatic rocks along the Motagua fault zone, Guatemala. *Ofioliti* **28**, 115–120.

Hermes, O. D. (1973). Paragenetic relationships in an amphibolitic tectonic block in the Franciscan Terrain, Panoche Pass, California. *Journal of Petrology* **14**, 1–32.

Holway, R. S. (1904). Eclogites in California. *Journal of Geology* **12**, 344–358.

Horodyskyj, U., Lee, C. & Luffi, P. (2009). Geochemical evidence for exhumation of eclogite via serpentinite channels in ocean–continent subduction zones. *Geosphere* **5**, 426–438.

Jamtveit, B. & Hervig, R. L. (1994). Constraints on transport and kinetics in hydrothermal systems from zoned garnet crystals. *Science* **263**, 505–508.

Jamtveit, B., Wogelius, R. A. & Fraser, D. G. (1993). Zonation patterns of skarn garnets—records of hydrothermal system evolution. *Geology* **21**, 113–116.

Johnson, C. & Harlow, G. (1999). Guatemala jadeitites and albitites were formed by deuterium-rich serpentinizing fluids deep within a subduction zone. *Geology* **27**, 629.

Kelly, J. L., Fu, B., Kita, N. T. & Valley, J. W. (2007). Optically continuous silcrete quartz cements of the St. Peter Sandstone: High precision oxygen isotope analysis by ion microprobe. *Geochimica et Cosmochimica Acta* **71**, 3812–3832.

Kelly, N. M. & Harley, S. L. (2005). An integrated microtextural and chemical approach to zircon geochronology: refining the Archaean history of the Napier Complex, east Antarctica. *Contributions to Mineralogy and Petrology* **149**, 57–84.

Kerrick, D. M. & Connolly, J. A. D. (2001). Metamorphic devolatilization of subducted marine sediments and the transport of volatiles into the Earth's mantle. *Nature* **411**, 293.

King, R. L., Kohn, M. & Eiler, J. (2003). Constraints on the petrologic structure of the subduction zone slab–mantle interface from Franciscan Complex exotic ultramafic blocks. *Geological Society of America Bulletin* **115**, 1097–1109.

King, R. L., Bebout, G. E., Moriguti, T. & Nakamura, E. (2006). Elemental mixing systematics and Sr–Nd isotope geochemistry of melange formation: Obstacles to identification of fluid sources to arc volcanics. *Earth and Planetary Science Letters* **246**, 288–304.

King, R. L., Bebout, G. E., Grove, M., Moriguti, T. & Nakamura, E. (2007). Boron and lead isotope signatures of subduction-zone melange formation: Hybridization and fractionation along the slab–mantle interface beneath volcanic arcs. *Chemical Geology* **239**, 305–322.

Kita, N. T., Ushikubo, T., Fu, B. & Valley, J. W. (2009). High precision SIMS oxygen isotope analysis and the effect of sample topography. *Chemical Geology* **264**, 43–57.

Kohn, M. J. & Valley, J. W. (1998*a*). Oxygen isotope geochemistry of the amphiboles: Isotope effects of cation substitutions in minerals. *Geochimica et Cosmochimica Acta* **62**, 1947–1958.

Kohn, M. J. & Valley, J. W. (1998*b*). Effects of cation substitutions in garnet and pyroxene on equilibrium oxygen isotope fractionations. *Journal of Metamorphic Geology* **16**, 625–639.

Kohn, M. J., Valley, J. W., Elsenheimer, D. & Spicuzza, M. J. (1993). Isotope zoning in garnet and staurolite; evidence for closed-system

mineral growth during regional metamorphism. *American Mineralogist* **78**, 988–1001.

Krogh, E. J. (1982). Metamorphic evolution of Norwegian country-rock eclogites, as deduced from mineral inclusions and compositional zoning in garnets. *Lithos* **15**, 305–321.

Krogh, E. J., Oh, C. W. & Liou, J. G. (1994). Polyphase and anticlockwise *P–T* evolution for Franciscan eclogites and blueschists from Jenner, California, USA. *Journal of Metamorphic Geology* **12**, 121–134.

Krogh, T. E., Mysen, B. O. & Davis, G. L. (1974). A Paleozoic age for the primary minerals of a Norwegian eclogite. *Carnegie Institution of Washington Yearbook* **73**, 575–576.

Lancaster, P. J., Fu, B., Page, F. Z., Kita, N. T., Bickford, M. E., Hill, B. M., McLelland, J. M. & Valley, J. W. (2009). Genesis of metapelitic migmatites in the Adirondack Mountains, New York. *Journal of Metamorphic Geology* **27**, 41–54.

Li, X.-P., Zhang, L.-F., Wilde, S. A., Song, B. & Liu, X.-M. (2010). Zircons from rodingite in the Western Tianshan serpentinite complex: Mineral chemistry and U–Pb ages define nature and timing of rodingitization. *Lithos* **118**, 17–34.

Liati, A. & Gebauer, D. (1999). Constraining the prograde and retrograde *P–T–t* path of Eocene HP rocks by SHRIMP dating of different zircon domains: inferred rates of heating, burial, cooling and exhumation for central Rhodope, northern Greece. *Contributions to Mineralogy and Petrology* **135**, 340–354.

Ludwig, K. R. (2003). *ISOPLOT EX Version 3. Berkeley Geochronology Center Special Publication* **4**, .

Marschall, H. R. & Schumacher, J. C. (2012). Arc magmas sourced from mélange diapirs in subduction zones. *Nature Geoscience* **5**, 862–867.

Martin, L. A. J., Duchene, S., Deloule, E. & Vanderhaeghe, O. (2006). The isotopic composition of zircon and garnet: A record of the metamorphic history of Naxos, Greece. *Lithos* **87**, 174–192.

Martin, L. A., Ballèvre, M., Boulvais, P., Halfpenny, A., Vanderhaeghe, O., Duchêne, S. & Deloule, E. (2011*a*). Garnet re-equilibration by coupled dissolution–reprecipitation: evidence from textural, major element and oxygen isotope zoning of 'cloudy' garnet. *Journal of Metamorphic Geology* **29**, 213–231.

Martin, L. A. J., Rubatto, D., Vitale Brovarone, A. & Hermann, J. (2011*b*). Late Eocene lawsonite–eclogite facies metasomatism of a granulite sliver associated to ophiolites in Alpine Corsica. *Lithos* **125**, 620–640.

Mattinson, J. M. (1986). Geochronology of high-pressure–low-temperature Franciscan metabasite: a new approach using the U–Pb system. In: Evans, B. W. & Brown, E. H. (eds) *Blueschists and Eclogites. Geological Society of America, Memoirs* **164**, 95–105.

Moller, A. & Kennedy, A. (2006). Extremely high Th/U in metamorphic zircon: In situ dating of the Labwor Hills granulites. *Geochimica et Cosmochimica Acta* **70**, A425.

Moore, D. E. (1984). Metamorphic history of a high-grade blueschist exotic block from the Franciscan Complex, California. *Journal of Petrology* **25**, 126–150.

Moore, D. E. & Blake, M. C., Jr (1989). New evidence for polyphase metamorphism of glaucophane schist and eclogite exotic blocks in the Franciscan Complex, California and Oregon. *Journal of Metamorphic Geology* **7**, 211–228.

Mori, Y., Orihashi, Y., Miyamoto, T., Shimada, K., Shigeno, M. & Nishiyama, T. (2011). Origin of zircon in jadeitite from the Nishisonogi metamorphic rocks, Kyushu, Japan. *Journal of Metamorphic Geology* **29**, 673–684.

Mulcahy, S. R., King, R. L. & Vervoort, J. D. (2009). Lawsonite Lu–Hf geochronology: A new geochronometer for subduction zone processes. *Geology* **37**, 987–990.

Nadeau, S., Philippot, P. & Pineau, F. (1993). Fluid inclusion and mineral isotopic compositions (H–C–O) in eclogitic rocks as tracers of local fluid migration during high-pressure metamorphism. *Earth and Planetary Science Letters* **114**, 431–448.

Nelson, B. K. (1991). Sediment-derived fluids in subduction zones: isotopic evidence from veins in blueschist and eclogite of the Franciscan Complex, California. *Geology* **19**, 1033–1036.

Oh, C. W. & Liou, J. G. (1990). Metamorphic evolution of two different eclogites in the Franciscan Complex, California, USA. *Lithos* **25**, 41–53.

Paces, J. B. & Miller, J. D., Jr (1993). Precise U–Pb ages of Duluth Complex and related mafic intrusions, northeastern Minnesota: geochronological insights to physical, petrogenetic, paleomagnetic, and tectonomagmatic processes associated with the 1·1 Ga Midcontinent Rift System. *Journal of Geophysical Research, B, Solid Earth and Planets* **98**, 13997–14013.

Page, F. Z., Essene, E. J. & Mukasa, S. B. (2003). Prograde and retrograde history of eclogites from the Eastern Blue Ridge, North Carolina, USA. *Journal of Metamorphic Geology* **21**, 685–698.

Page, F. Z., Armstrong, L. S., Essene, E. J. & Mukasa, S. B. (2007*a*). Prograde and retrograde history of the Junction School eclogite, California, and an evaluation of garnet–phengite–clinopyroxene thermobarometry. *Contributions to Mineralogy and Petrology* **153**, 533–555.

Page, F. Z., Fu, B., Kita, N. T., Fournelle, J., Spicuzza, M. J., Schulze, D. J., Viljoen, F., Basei, M. A. & Valley, J. W. (2007*b*). Zircons from kimberlite: New insights from oxygen isotopes, trace elements, and Ti in zircon thermometry. *Geochimica et Cosmochimica Acta* **71**, 3887–3903.

Page, F. Z., Ushikubo, T., Kita, N. T., Riciputi, L. R. & Valley, J. W. (2007*c*). High-precision oxygen isotope analysis of picogram samples reveals 2 μm gradients and slow diffusion in zircon. *American Mineralogist* **92**, 1772–1775.

Page, F. Z., Kita, N. T. & Valley, J. W. (2010). Ion microprobe analysis of oxygen isotopes in garnets of complex chemistry. *Chemical Geology* **270**, 9–19.

Peacock, S. M. (1990). Fluid processes in subduction zones. *Science* **248**, 329–337.

Philippot, P. (1993). Fluid–melt–rock interaction in mafic eclogites and coesite-bearing metasediments: constraints on volatile recycling during subduction. *Chemical Geology* **108**, 93–112.

Philippot, P. & Selverstone, J. (1991). Trace-element-rich brines in eclogitic veins: implications for fluid composition and transport during subduction. *Contributions to Mineralogy and Petrology* **106**, 417–430.

Pincus, M. R., Page, F. Z., Spicuzza, M. J. & Valley, J. W. (2010). Widespread oxygen isotope disequilibrium in Franciscan high-grade blocks. *Geological Society of America, Abstracts with Programs* **42**, 629.

Putlitz, B., Matthews, A. & Valley, J. W. (2000). Oxygen and hydrogen isotope study of high-pressure metagabbros and metabasalts (Cyclades, Greece): implications for the subduction of oceanic crust. *Contributions to Mineralogy and Petrology* **138**, 114–126.

Putlitz, B., Katzir, Y., Matthews, A. & Valley, J. W. (2001). Oceanic and orogenic fluid–rock interaction in $^{18}O/^{16}O$-enriched metagabbros of an ophiolite (Tinos, Cyclades). *Earth and Planetary Science Letters* **193**, 99–113.

Quidelleur, X., Grove, M., Lovera, O. M., Harrison, T. M., Yin, A. & Ryerson, F. J. (1997). Thermal evolution and slip history of the Renbu Zedong Thrust, southeastern Tibet. *Journal of Geophysical Research, B, Solid Earth and Planets* **102**, 2659–2679.

Raimondo, T., Clark, C., Hand, M., Cliff, J. & Harris, C. (2012). High-resolution geochemical record of fluid–rock interaction in a

mid-crustal shear zone: a comparative study of major element and oxygen isotope transport in garnet. *Journal of Metamorphic Geology* **30**, 255–280.

Ravna, E. J. K. & Terry, M. P. (2004). Geothermobarometry of UHP and HP eclogites and schists—an evaluation of equilibria among garnet–clinopyroxene–kyanite–phengite–coesite/quartz. *Journal of Metamorphic Geology* **22**, 579–592.

Ross, J. A. & Sharp, W. D. (1986). $^{40}Ar/^{39}Ar$ and Sm/Nd dating of garnet amphibolite in the Coast Ranges, California. *EOS Transactions, American Geophysical Union* **67**, 1249.

Ross, J. A. & Sharp, W. D. (1988). The effects of sub-blocking temperature metamorphism on the K/Ar systematics of hornblendes: $^{40}Ar/^{39}Ar$ dating of polymetamorphic garnet amphibolite from the Franciscan Complex, California. *Contributions to Mineralogy and Petrology* **100**, 213–221.

Rubatto, D. (2002). Zircon trace element geochemistry; partitioning with garnet and the link between U–Pb ages and metamorphism. *Chemical Geology* **184**, 123–138.

Rubatto, D. & Hermann, J. (2003). Zircon formation during fluid circulation in eclogites (Monviso, Western Alps): implications for Zr and Hf budget in subduction zones. *Geochimica et Cosmochimica Acta* **67**, 2173–2187.

Rubatto, D., Gebauer, D. & Compagnoni, R. (1999). Dating of eclogite-facies zircons: the age of Alpine metamorphism in the Sesia–Lanzo Zone (Western Alps). *Earth and Planetary Science Letters* **167**, 141–158.

Rubatto, D., Müntener, O., Barnhoorn, A. & Gregory, C. (2008). Dissolution–reprecipitation of zircon at low-temperature, high-pressure conditions (Lanzo Massif, Italy). *American Mineralogist* **93**, 1519–1529.

Rubatto, D., Regis, D., Hermann, J., Boston, K., Engi, M., Beltrando, M. & McAlpine, S. R. B. (2011). Yo-yo subduction recorded by accessory minerals in the Italian Western Alps. *Nature Geoscience* **4**, 1–5.

Russell, A. K. (2011). Oxygen isotopes in garnet from eclogite: oxygen isotope geochemistry of the Bohemian Massif and zoning revealed by secondary ion mass spectrometry. MS thesis, University of Wisconsin–Madison, 291 p.

Russell, A. K., Kitajima, K., Strickland, A., Medaris, L .G., Jr, Spicuzza, M. J. & Valley, J. W. (2013). Eclogite-facies fluid infiltration revealed by $\delta^{18}O$ zoning in garnet. *Contributions to Mineralogy and Petrology* **164**, 103–116.

Sadofsky, S. & Bebout, G. E. (2001). Paleohydrogeology at 5- to 50-kilometer depths of accretionary prisms: The Franciscan Complex, California. *Geophysical Research Letters* **28**, 2309–2312.

Scambelluri, M. & Philippot, P. (2001). Deep fluids in subduction zones. *Lithos* **55**, 213–227.

Schmitz, M. D. & Bowring, S. A. (2001). The significance of U–Pb zircon dates in lower crustal xenoliths from the southwestern margin of the Kaapvaal Craton, Southern Africa. *Chemical Geology* **172**, 59–76.

Schmitz, M. D., Bowring, S. A. & Ireland, T. R. (2003). Evaluation of Duluth Complex anorthositic series (AS3) zircon as a U–Pb geochronological standard: New high-precision isotope dilution thermal ionization mass spectrometry results. *Geochimica et Cosmochimica Acta* **67**, 3665–3672.

Selverstone, J., Franz, G., Thomas, S. & Getty, S. (1992). Fluid variability in 2 GPa eclogites as an indicator of fluid behavior during subduction. *Contributions to Mineralogy and Petrology* **112**, 341–357.

Skelton, A., Annersten, H. & Valley, J. (2002). $\delta^{18}O$ and yttrium zoning in garnet: time markers for fluid flow? *Journal of Metamorphic Geology* **20**, 457–466.

Sobolev, N. V., Schertl, H.-P., Valley, J. W., Page, F. Z., Kita, N. T., Spicuzza, M. J., Neuser, R. D. & Logvinova, A. M. (2011). Oxygen isotope variations of garnets and clinopyroxenes in a layered diamondiferous calcsilicate rock from Kokchetav Massif, Kazakhstan: a window into the geochemical nature of deeply subducted UHPM rocks. *Contributions to Mineralogy and Petrology* **162**, 1079–1092.

Sorensen, S. S. & Grossman, J. N. (1989). Enrichment of trace elements in garnet amphibolites from a paleo-subduction zone: Catalina Schist, Southern California. *Geochimica et Cosmochimica Acta* **53**, 3155–3177.

Sorensen, S. S., Grossman, J. N. & Perfit, M. R. (1997). Phengite-hosted LILE enrichment in eclogite and related rocks; implications for fluid-mediated mass transfer in subduction zones and arc magma genesis. *Journal of Petrology* **38**, 3–34.

Sorensen, S. S., Harlow, G. E. & Rumble, D. (2006). The origin of jadeitite-forming subduction-zone fluids: CL-guided SIMS oxygen-isotope and trace-element evidence. *American Mineralogist* **91**, 979–996.

Spandler, C. & Hermann, J. (2005). High-pressure veins in eclogite from New Caledonia; Implications for fluid migration and seismic activity in subduction zones. *Geochimica et Cosmochimica Acta* **69**, A664.

Spandler, C., Pettke, T. & Rubatto, D. (2011). Internal and external fluid sources for eclogite-facies veins in the Monviso meta-ophiolite, Western Alps: Implications for fluid flow in subduction zones. *Journal of Petrology* **52**, 1207–1236.

Spicuzza, M. J., Valley, J. W. & McConnell, V. S. (1998). Oxygen isotope analysis of whole rock via laser fluorination: An air-lock approach. *Geological Society of America, Abstracts with Programs* **30**, 80.

Trail, D., Watson, E. B. & Tailby, N. D. (2011). The oxidation state of Hadean magmas and implications for early Earth's atmosphere. *Nature* **480**, 79–82.

Trail, D., Watson, E. B. & Tailby, N. D. (2012). Ce and Eu anomalies in zircon as proxies for the oxidation state of magmas. *Geochimica et Cosmochimica Acta* **97**, 70–87.

Tsujimori, T., Liou, J. G., Wooden, J. L. & Miyamoto, T. (2005). U-Pb Dating of large Zircons in low-temperature Jadeitite from the osayama serpentinite mélange, Southwest Japan: Insights into the timing of serpentinization. *International Geology Review* **47**, 1–10.

Tsujimori, T., Matsumoto, K., Wakabayashi, J. & Liou, J. G. (2006*a*). Franciscan eclogite revisited: Reevaluation of the P–T evolution of tectonic blocks from Tiburon Peninsula, California, U.S.A. *Mineralogy and Petrology* **88**, 243–267.

Tsujimori, T., Sisson, V., Liou, J. G., Harlow, G. E. & Sorensen, S. S. (2006*b*). Very-low-temperature record of the subduction process: A review of worldwide lawsonite eclogites. *Lithos* **92**, 609–624.

Valley, J. W. (2003). Oxygen isotopes in zircon. In: Hanchar, J. M. & Hoskin, P. W. O. (eds) *Zircon. Mineralogical Society of America and Geochemical Society, Reviews in Mineralogy and Geochemistry* **53**, 343–385.

Valley, J. W. & Kita, N. T. (2009). *In situ* oxygen isotope geochemistry by ion microprobe. In: Fayek, M. (ed.) *Secondary Ion Mass Spectrometry in the Earth Sciences. Mineralogical Association of Canada, Short Courses* **41**, 19–63.

Valley, J. W., Chiarenzelli, J. R. & McLelland, J. M. (1994). Oxygen isotope geochemistry of zircon. *Earth and Planetary Science Letters* **126**, 187–206.

Valley, J. W., Kitchen, N., Kohn, M. J., Niendorf, C. R. & Spicuzza, M. J. (1995). UWG-2, a garnet standard for oxygen isotope ratios: strategies for high precision and accuracy with laser heating. *Geochimica et Cosmochimica Acta* **59**, 5223–5231.

Valley, J. W., Kinny, P. D., Schulze, D. J. & Spicuzza, M. J. (1998). Zircon megacrysts from kimberlite: oxygen isotope variability

among mantle melts. *Contributions to Mineralogy and Petrology* **133**, 1–11.

Valley, J. W., Bindeman, I. N. & Peck, W. H. (2003). Empirical calibration of oxygen isotope fractionation in zircon. *Geochimica et Cosmochimica Acta* **67**, 3257–3266.

Vielzeuf, D., Veschambre, M. & Brunet, F. (2005). Oxygen isotope heterogeneities and diffusional profiles in composite metamorphic/magmatic garnets from the Pyrenees. *American Mineralogist* **90**, 463–472.

Wakabayashi, J. (1990). Counterclockwise *P–T–t* paths from amphibolites, Franciscan Complex, California: relics from the early stages of subduction zone metamorphism. *Journal of Geology* **98**, 657–680.

Wakabayashi, J. (2012). Subducted sedimentary serpentinite mélanges: Record of multiple burial–exhumation cycles and subduction erosion. *Tectonophysics* **568–569**, 230–247.

Wakabayashi, J. & Dumitru, T. A. (2007). $^{40}Ar/^{39}Ar$ ages from coherent, high-pressure metamorphic rocks of the Franciscan complex, California: Revisiting the timing of metamorphism of the world's type subduction complex. *International Geology Review* **49**, 873–906.

Watson, E. B. & Cherniak, D. (1997). Oxygen diffusion in zircon. *Earth and Planetary Science Letters* **148**, 527–544.

Wiedenbeck, M., Allé, P., Corfu, F., Griffin, W. L., Meier, M., Oberli, F., von Quadt, A., Roddick, J. C. & Spiegel, W. (1995). Three natural zircon standards for U–Th–Pb, Lu–Hf, trace element and REE analyses. *Geostandards Newsletter* **19**, 1–23.

Wiedenbeck, M., Hanchar, J. M., Peck, W. H. *et al.* (2004). Further characterisation of the 91500 zircon crystal. *Geostandards and Geoanalytical Research* **28**, 9–39.

Yang, P. & Rivers, T. (2003). The origin of Mn and Y annuli in garnet and the thermal dependence of P in garnet and Y in apatite in calc-pelite and pelite, Gagnon terrane, western Labrador. *Geological Materials Research* **4**, 1–35.

Yui, T.-F., Maki, K., Usuki, T., Lan, C.-Y., Martens, U., Wu, C.-M., Wu, T.-W. & Liou, J. G. (2010). Genesis of Guatemala jadeitite and related fluid characteristics: Insight from zircon. *Chemical Geology* **270**, 45–55.

Yui, T.-F., Maki, K., Wang, K.-L., Lan, C.-Y., Usuki, T., Iizuka, Y., Wu, C.-M., Wu, T.-W., Nishiyama, T., Martens, U., Liou, J. G. & Grove, M. (2012). Hf isotope and REE compositions of zircon from jadeitite (Tone, Japan and north of the Motagua fault, Guatemala): implications on jadeitite genesis and possible protoliths. *European Journal of Mineralogy* **24**, 263–275.